

Modeling GW170817 based on numerical relativity and its implicationsMasaru Shibata,¹ Sho Fujibayashi,¹ Kenta Hotokezaka,^{2,1} Kenta Kiuchi,¹ Koutarou Kyutoku,^{3,1}
Yuichiro Sekiguchi,^{4,1} and Masaomi Tanaka⁵¹*Center for Gravitational Physics, Yukawa Institute for Theoretical Physics, Kyoto University,
Kyoto 606-8502, Japan*²*School of Natural Sciences, Institute for Advanced Study, Princeton, New Jersey 08540, USA*³*Theory Center, Institute of Particle and Nuclear Studies, KEK, Tsukuba 305-0801, Japan;
Department of Particle and Nuclear Physics, the Graduate University for Advanced Studies (Sokendai),
Tsukuba 305-0801, Japan;
and Interdisciplinary Theoretical Science (iTHES) Research Group,
RIKEN, Wako, Saitama 351-0198, Japan*⁴*Department of Physics, Toho University, Funabashi, Chiba 274-8510, Japan*⁵*National Astronomical Observatory of Japan, Mitaka, Tokyo 181-8588, Japan
(Received 24 October 2017; published 22 December 2017)*

Gravitational-wave observation together with a large number of electromagnetic observations shows that the source of the latest gravitational-wave event, GW170817, detected primarily by advanced LIGO, is the merger of a binary neutron star. We attempt to interpret this observational event based on our results of numerical-relativity simulations performed so far, paying particular attention to the optical and infrared observations. We finally reach a conclusion that this event is described consistently by the presence of a long-lived hypermassive or supramassive neutron star as the merger remnant because (i) significant contamination by lanthanide elements along our line of sight to this source can be avoided by the strong neutrino irradiation from it and (ii) it could play a crucial role in producing an ejecta component of appreciable mass with fast motion in the postmerger phase. We also point out that (I) the neutron-star equation of state has to be sufficiently stiff (i.e., the maximum mass of cold spherical neutron stars, M_{max} , has to be appreciably higher than $2 M_{\odot}$) in order for a long-lived massive neutron star to be formed as the merger remnant for the binary systems of GW170817, for which the initial total mass is $\gtrsim 2.73 M_{\odot}$, and (II) the absence of optical counterparts associated with relativistic ejecta suggests a not-extremely-high value of M_{max} approximately as $2.15\text{--}2.25 M_{\odot}$.

DOI: [10.1103/PhysRevD.96.123012](https://doi.org/10.1103/PhysRevD.96.123012)**I. INTRODUCTION**

On August 17, 2017, two advanced LIGO detectors (with important assistance by advanced VIRGO) succeeded in the first direct detection of gravitational waves from an inspiraling binary system of two neutron stars, which is referred to as GW170817 [1]. The data analysis for this gravitational-wave event derives that the chirp mass, defined by $\mathcal{M} := (m_1 m_2)^{3/5} / (m_1 + m_2)^{1/5}$ [where m_1 and $m_2 (\leq m_1)$ denote each mass of the binary], is $\approx 1.188_{-0.002}^{+0.004} M_{\odot}$ for the 90% credible interval. This implies that the total mass $m := m_1 + m_2 = 2.729(\eta/0.25)^{-3/5} M_{\odot} \geq 2.729 M_{\odot}$. Here, η denotes the symmetric mass ratio defined by $\eta := m_1 m_2 / m^2 (\leq 0.25)$. The mass ratio of the binary is not well constrained as 0.7–1.0 within the 90% credible interval under the assumption that the dimensionless spin of each neutron star is reasonably small (≤ 0.05). However, the values of η for this mass-ratio range are between 0.242 and 0.250. This implies that the total mass is well constrained in the range between $\approx 2.73 M_{\odot}$ and $\approx 2.78 M_{\odot}$ for the 90% credible interval.

The luminosity distance to the source from the Earth is approximately $D = 40_{-14}^{+8}$ Mpc [1], and follow-up optical

observations (e.g., Ref. [2] for a summary) found a counterpart of this event and identified a lenticular galaxy, NGC 4993, as the host galaxy. Since the sky location is accurately determined and the total signal-to-noise ratio (SNR) of the gravitational-wave signal is as high as 32.4 [1], the inclination angle of the binary orbital axis with respect to our line of sight is constrained to be $\iota \lesssim 28^\circ$ [1], and the effective distance to the source (after taking into account the orbital inclination and sky location with respect to the detector's orbital planes) is estimated to be $D_{\text{eff}} \approx 57$ Mpc [1].

A large number of observations in the optical and IR bands have been also carried out following the gravitational-wave detection (e.g., Refs. [3–14]). These observations show that the emission properties are largely consistent with the macronova/kilonova model [15,16], suggesting that high-velocity, neutron-rich matter of mass 0.01–0.1 M_{\odot} ejected from the neutron-star mergers radioactively shines through the r -process nucleosynthesis [17,18] in the optical-IR bands for 0.5–20 days after the merger, and that the spectrum is broadly consistent with the quasithermal spectrum with significant reddening. However, (i) the peak time of the light curve is earlier than the expectation from a

macronova/kilonova model in which heavy r -process elements are appreciably synthesized and the typical value of the opacity is expected to be $\kappa \approx 10 \text{ cm}^2/\text{g}$ due to the appreciable presence of lanthanide elements [19–22], and (ii) the peak luminosity is higher than what the typical scenarios have predicted for the dynamical ejecta of binary neutron-star mergers. A naive interpretation for these observational results is that a fraction of the ejecta is composed of lanthanide-poor material and the total ejecta mass would be $\sim 0.025\text{--}0.05 M_\odot$ [3–13], which is somewhat larger than the typical dynamical ejecta mass of $\sim 0.001\text{--}0.01 M_\odot$ obtained by numerical-relativity simulations for binary neutron-star mergers.

In this paper, we attempt to interpret the results of the electromagnetic observations for the optical-IR bands in terms of the results of our wide variety of numerical-relativity simulations performed so far. Numerical-relativity simulations for the merger of binary neutron stars have been performed in our group since 1999 [23,24], and now, detailed modeling for this phenomenon is feasible, as we describe in this paper. We thus use the latest numerical-relativity results for the interpretation of the GW170817 event.

Fermi GBM and INTEGRAL reported a possible detection of an extremely weak short gamma-ray burst of 2 s duration and the (isotropic) luminosity $\sim 10^{47} \text{ erg/s}$ at $\sim 1.7 \text{ s}$ after the trigger of the GW170817 event [25–27]. Since the binary orbital axis with respect to our line of sight is likely to be mildly misaligned with $i \lesssim 28^\circ$ [1], this observation suggests a detection of an off-axis gamma-ray burst emission or cocoon emission arising from an ultrarelativistic jet launched at the merger [28,29]. However, the production of such an ultrarelativistic jet in numerical-relativity simulations is beyond the scope of our paper. Thus, we focus on interpreting the optical and IR data in the following.

The paper is organized as follows. In Sec. II, we summarize possible scenarios for the merger processes of binary neutron stars with the total mass $m = 2.7\text{--}2.8 M_\odot$ and mass ratio $q = m_2/m_1 = 0.8\text{--}1.0$ in the current constraint for the neutron-star equation of state (EOS). We note that there are seven Galactic compact binary neutron stars observed to date [30]. The mass ratio of these binaries is in the range between ≈ 0.75 and ≈ 1 , and the dimensionless spin of neutron stars, for which the spin period is measured, is smaller than 0.03. Thus, in this paper, we do not consider extreme cases with small mass ratios like ≤ 0.7 or with a rapidly spinning neutron star. We then discuss in Sec. III what the special features for the observations of GW170817 are and draw a conclusion that the key point for describing this event is the presence of a long-lived massive neutron star (either a hypermassive or supramassive neutron star, see Refs. [31,32] for their definition) as the remnant of the binary neutron-star merger because significant contamination by lanthanide elements along our line of sight to this source can be avoided by the strong neutrino irradiation from it and also because it could

play a crucial role in producing an ejecta component of appreciable mass with the fast motion of the velocity $\sim 0.1\text{--}0.2c$. We also point out that if the long-lived massive neutron star is indeed formed this implies that the EOS has to be stiff enough (i.e., the maximum mass of cold spherical neutron stars has to be high enough) to escape the formation of a black hole in a short time scale after the merger for the system of total mass $m \gtrsim 2.73 M_\odot$. Section IV is devoted to discussing implications of GW170817 and perspectives for the future observation. We then summarize this paper in Sec. V. Throughout this paper, c denotes the speed of light.

II. SUMMARY OF NUMERICAL-RELATIVITY RESULTS

In this section, we summarize the possible merger and postmerger processes, in particular focusing on the merger remnant, ejecta mass, and electron fraction of the ejecta. The first one is closely related to the central energy source, which determines the mechanisms of mass ejection. The latter two are the key quantities for describing the properties of the electromagnetic signals associated with the mass ejection. In the following subsections, we first summarize the merger process of binary neutron stars and its dependence on the EOS employed, total mass, and mass ratio of a binary focusing on the first $\sim 30 \text{ ms}$ after the onset of merger. Then, we discuss the possible long-term evolution processes of the merger remnants and the associated mass ejection. The emphasis is on the following point: the merger process, postmerger remnant evolution, mass ejection process, and properties of the ejecta depend strongly on the neutron-star EOS, in particular, on the maximum mass of cold spherical neutron stars, M_{max} .

A. Dynamical merger process and dynamical mass ejection

A number of numerical-relativity simulations (e.g., Refs. [33–41]) have shown that the merger process and remnant object depend strongly on the EOS of neutron stars, which is still poorly constrained. However, because we approximately know the total mass of the binary system for the event GW170817, we can discuss in detail the possible merger process and remnant for a given hypothetical EOS. In the following, we describe typical scenarios for the cases of soft and stiff EOS, for which the maximum masses for the cold spherical neutron stars are $M_{\text{max}} \lesssim 2.1 M_\odot$ and $\gtrsim 2.2 M_\odot$, respectively. Popular soft and stiff EOS, which are often employed in the community of numerical relativity, are SFHo [42] and DD2 EOS [43], for which $R \approx 11.9$ and 13.2 km and $M_{\text{max}} = 2.06 M_\odot$ and $2.42 M_\odot$, respectively (see Table I). Thus, we discuss the possible merger process and remnants picking up numerical-relativity results for these two representative EOS. We note that for these two EOS the typical radius and maximum mass

TABLE I. Equations of state employed; the maximum mass for cold spherical neutron stars, M_{\max} , in units of the solar mass; the radius, R_M ; and the dimensionless tidal deformability Λ_M of spherical neutron stars of gravitational mass $M = 1.20, 1.30, 1.40$, and $1.50 M_\odot$. R_M is listed in units of kilometers. The last five data points show the binary tidal deformability for $\eta = 0.250, 0.248, 0.246, 0.244$, and 0.242 with $\mathcal{M} = 1.19 M_\odot$.

| EOS | M_{\max} | $R_{1.20}$ | $R_{1.30}$ | $R_{1.40}$ | $R_{1.50}$ | $\Lambda_{1.20}$ | $\Lambda_{1.30}$ | $\Lambda_{1.40}$ | $\Lambda_{1.50}$ | Λ |
|------|------------|------------|------------|------------|------------|------------------|------------------|------------------|------------------|-------------------------|
| SFHo | 2.06 | 11.96 | 11.93 | 11.88 | 11.83 | 864 | 533 | 332 | 208 | 388, 387, 387, 386, 385 |
| DD2 | 2.42 | 13.14 | 13.18 | 13.21 | 13.24 | 1622 | 1053 | 696 | 467 | 797, 788, 780, 772, 764 |

are positively correlated. However, for some EOS like APR4 [44], the maximum mass could be $2.2 M_\odot$ even for $R < 12$ km. By contrast, for EOS like H4 [45], the maximum mass is often only slightly larger than $2 M_\odot$ while $R \sim 13.5$ km. In the discussion of this paper, the most important quantity is the maximum mass, M_{\max} , and the typical neutron-star radius, R , is not as important as the maximum mass. We will touch on this point in the final paragraphs of this subsection.

Table II summarizes the results of our numerical-relativity simulations for the total mass $m = 2.7\text{--}2.9 M_\odot$ in the SFHo and DD2 EOS. Several numerical results in this table are taken from Refs. [40,41]. These simulations were performed taking into account finite-temperature effects of nuclear-matter EOS, neutrino cooling, and neutrino heating. We note that including the neutrino heating (irradiation) is quite important for predicting the profile of the electron fraction, Y_e , for the merger remnants and ejecta, and hence, in the following, we refer only to the numerical-relativity work in which this effect is taken into account.

In this subsection, we focus only on the dynamical ejecta that are ejected in the first ~ 30 ms after the onset of merger.

In these simulations of the neutron-star mergers, no viscous nor magnetohydrodynamics (MHD) effects are taken into account. These are likely to play key roles for the long-term evolution of the merger remnants and could drive mass ejection in addition to the dynamical ejecta. In Table II, such ejecta components are not included. We will discuss the long-term evolution processes of the merger remnant in the next subsection (see Sec. II B).

I. Summary of the dynamical ejecta

Table II tells us the following facts:

- (i) For the SFHo models, hypermassive neutron stars are formed after the merger temporarily for the total mass of $m = 2.7\text{--}2.8 M_\odot$, but they subsequently collapse to a black hole surrounded by a torus (see Fig. 1). The lifetime of the hypermassive neutron stars is $\lesssim 10$ ms in this EOS model and is shorter for higher total mass; for $m = 2.8 M_\odot$, it is ~ 3 ms. The mass and spin of the remnant black holes are approximately $0.96m$ and 0.7 , respectively, for the mass ratio $q \gtrsim 0.8$. The torus mass depends strongly on q . However, for appreciably asymmetric binaries with $q \lesssim 0.93$, the torus mass is likely to be larger

TABLE II. Merger remnants and properties of dynamical ejecta for two finite-temperature neutron-star EOS, SFHo and DD2, and for the cases with different masses. The results of our radiation hydrodynamics simulations, in which both the neutrino heating and cooling are taken into account, are listed. The quantities for the remnants are determined at ≈ 30 ms after the onset of merger. HMNS, BH, and MNS denote hypermassive neutron star, black hole, and massive (hypermassive or supramassive) neutron star, respectively. The torus mass for the DD2 EOS is determined from the mass located outside the central region of MNS with density $\rho \leq 10^{13}$ g/cm³ (left) and $\leq 10^{12}$ g/cm³ (right). The values of mass are shown in units of M_\odot . The BH spin means the dimensionless spin of the remnant black hole. \bar{Y}_e and \bar{v}_{ej} are the average value of the electron fraction, Y_e , and average velocity of the dynamical ejecta, respectively. We note that Y_e is broadly distributed between ~ 0.05 and ~ 0.5 , irrespective of the models (see Refs. [40,41]). The ejecta mass has uncertainty by a factor of ~ 2 (see Appendix for a discussion).

| EOS | m_1 & m_2 | m_2/m_1 | Remnant | BH mass | BH spin | Torus mass | M_{ej} | \bar{Y}_e | \bar{v}_{ej}/c |
|------|---------------|-----------|-----------------------|---------|---------|------------|-----------------|-------------|-------------------------|
| SFHo | 1.35, 1.35 | 1.00 | HMNS \rightarrow BH | 2.59 | 0.69 | 0.05 | 0.011 | 0.31 | 0.22 |
| SFHo | 1.37, 1.33 | 0.97 | HMNS \rightarrow BH | 2.59 | 0.70 | 0.06 | 0.008 | 0.30 | 0.21 |
| SFHo | 1.40, 1.30 | 0.93 | HMNS \rightarrow BH | 2.58 | 0.67 | 0.09 | 0.006 | 0.27 | 0.20 |
| SFHo | 1.45, 1.25 | 0.86 | HMNS \rightarrow BH | 2.58 | 0.69 | 0.12 | 0.011 | 0.18 | 0.24 |
| SFHo | 1.55, 1.25 | 0.81 | HMNS \rightarrow BH | 2.69 | 0.76 | 0.07 | 0.016 | 0.13 | 0.25 |
| SFHo | 1.65, 1.25 | 0.76 | BH | 2.76 | 0.77 | 0.09 | 0.007 | 0.16 | 0.23 |
| DD2 | 1.35, 1.35 | 1.00 | MNS | ... | ... | 0.23, 0.13 | 0.002 | 0.30 | 0.16 |
| DD2 | 1.40, 1.30 | 0.93 | MNS | ... | ... | 0.23, 0.11 | 0.003 | 0.26 | 0.18 |
| DD2 | 1.45, 1.25 | 0.86 | MNS | ... | ... | 0.30, 0.19 | 0.005 | 0.20 | 0.19 |
| DD2 | 1.40, 1.40 | 1.00 | MNS | ... | ... | 0.17, 0.09 | 0.002 | 0.31 | 0.16 |

than $\sim 0.1 M_\odot$. For the high-mass torus, the typical electron fraction is low, $Y_e \sim 0.1$ (see the upper panel of Fig. 1), because the density of the torus is high with the maximum value of $\sim 10^{12} \text{g/cm}^3$, resulting in strong electron degeneracy and strong neutronization. It should be also noted that the outer region with $x \lesssim 100 \text{ km}$ is fairly neutron rich with $Y_e = 0.2\text{--}0.4$ for this case. The property of low values of Y_e is different from that in the presence of a massive neutron star; see item (ii) below. The reason for this is that the torus, which is the only source of the neutrino emission in this remnant system, is a weak neutrino emitter (in the absence of efficient viscous heating), and hence the neutrino irradiation is not efficient enough to increase the value of Y_e for the matter around the black hole (a possible effect of the viscous heating will be discussed in Sec. II B).

- (ii) For the DD2 models, a long-lived massive (perhaps supramassive) neutron star surrounded by a torus is universally formed for $m = 2.7\text{--}2.8 M_\odot$ (see Fig. 2).

The torus mass depends weakly on the mass ratio, and it is $\sim 0.2 M_\odot$ for $q \sim 1$ and $\sim 0.3 M_\odot$ for $q \sim 0.85$. The electron fraction for the high-density region of the torus is slightly higher than that in the torus surrounding a black hole found in the SFHo models because the matter in the torus experiences shock heating more efficiently around the massive neutron stars. A more remarkable fact is that in the outer region of the torus at $x \gtrsim 100 \text{ km}$ the electron fraction is quite high as $Y_e \gtrsim 0.25$ (see the upper panel of Fig. 2) because of the irradiation by neutrinos emitted from the central massive neutron star and surrounding torus (e.g., Refs. [40,41,46,47]); in such an environment, the neutrino capture processes, $n + \nu_e \rightarrow p + e^-$ and $p + \bar{\nu}_e \rightarrow n + e^+$, take place quite efficiently in the matter surrounding the massive neutron star and torus, and by the balance of these reactions, the fraction of neutrons and protons approaches an equilibrium value in which the value of Y_e is

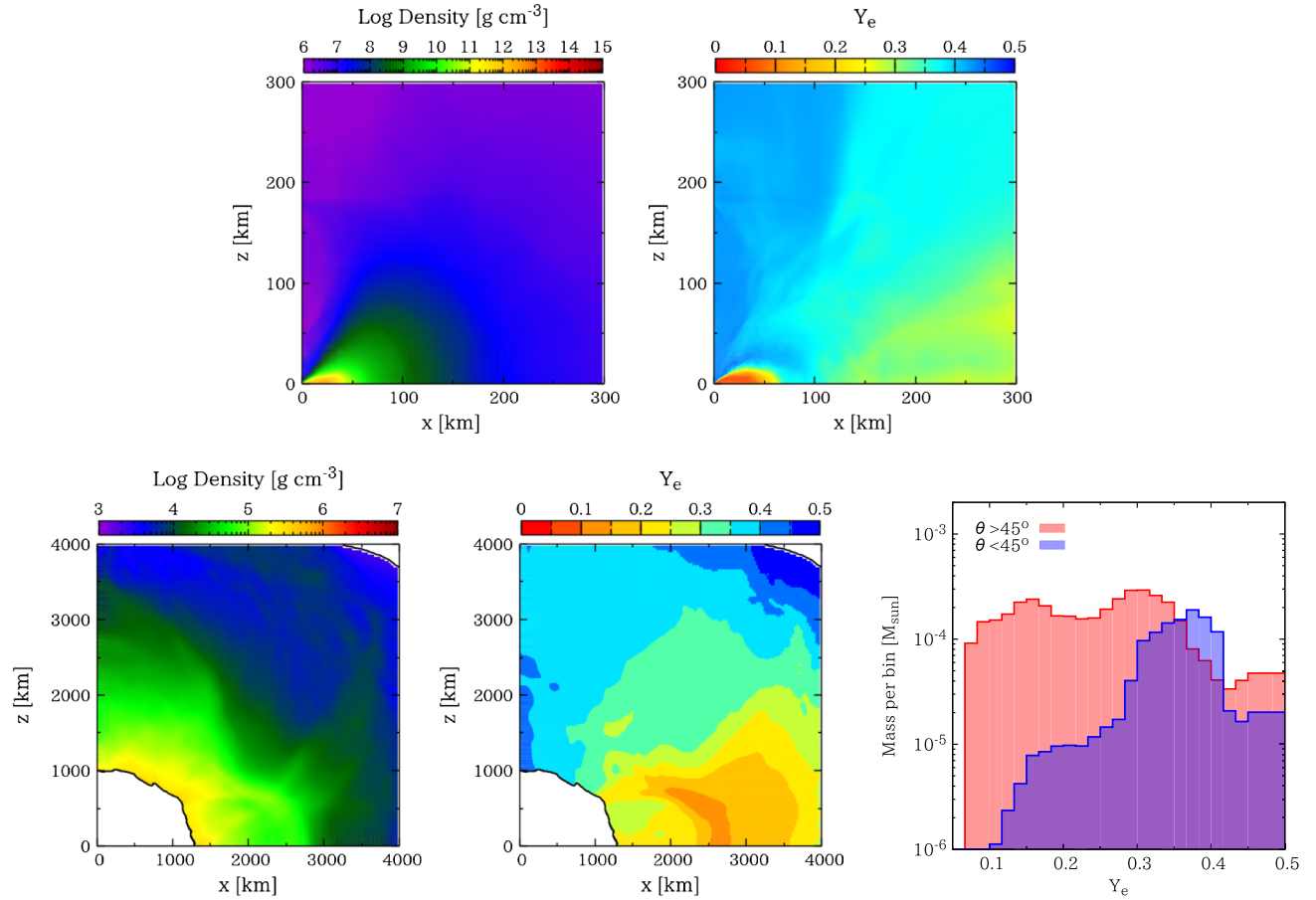


FIG. 1. Merger remnant for the SFHo EOS with $(m_1, m_2) = (1.4 M_\odot, 1.3 M_\odot)$. The upper left and right panels show the profiles of the rest-mass density and electron fraction for the merger remnant, i.e., a black hole surrounded by a torus, respectively. The lower left and middle panels show the profiles of the rest-mass density and electron fraction for the dynamical ejecta component, respectively. The white region in these panels indicates that no ejecta component is present in the inner region. These snapshots are generated at $\approx 40 \text{ ms}$ after the onset of merger. The lower right panel shows the mass histogram of the ejecta component as a function of Y_e for the regions of $z > x$ ($\theta < 45^\circ$) and $z < x$ ($\theta > 45^\circ$).

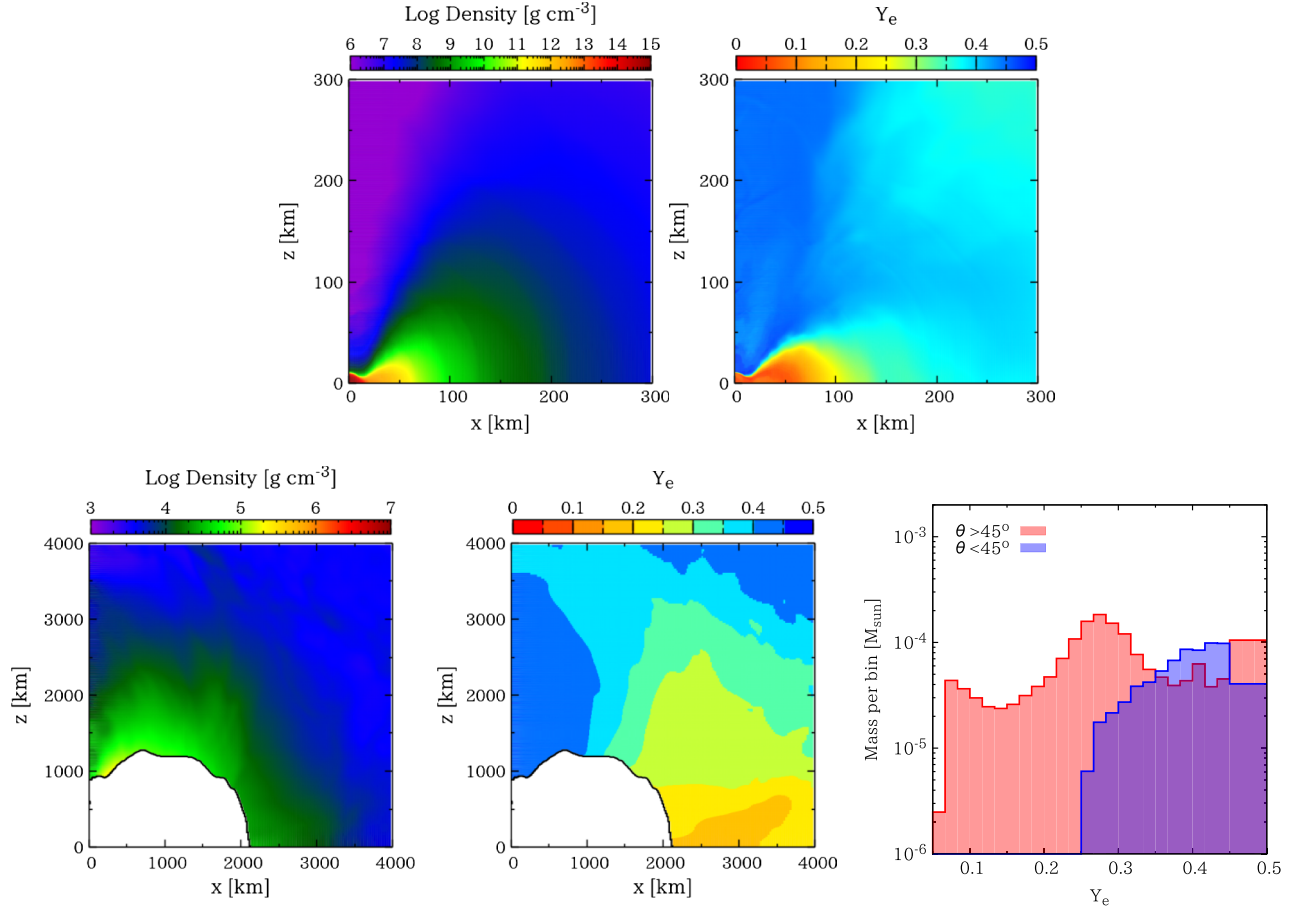


FIG. 2. The same as Fig. 1 but for the merger remnant for the DD2 EOS with $(m_1, m_2) = (1.4 M_\odot, 1.3 M_\odot)$. The snapshots are generated at ≈ 80 ms after the onset of merger. For this case, a massive neutron star is located at the center (compare the upper panels of Figs. 1 and 2).

enhanced to be $\lesssim 0.5$ and approximately given by (e.g., Ref. [48])

$$Y_{e,\text{eq}} \sim \left[1 + \frac{L_{\bar{\nu}_e} \cdot \langle \epsilon_{\bar{\nu}_e} \rangle - 2\Delta}{L_{\nu_e} \cdot \langle \epsilon_{\nu_e} \rangle + 2\Delta} \right]^{-1}, \quad (2.1)$$

where $\Delta = 1.293$ MeV (the mass energy difference between neutron and proton); $\langle \epsilon_{\nu_e} \rangle \approx 10$ MeV and $\langle \epsilon_{\bar{\nu}_e} \rangle \approx 15$ MeV denote the averaged neutrino energy of ν_e and $\bar{\nu}_e$, respectively; and L_{ν_e} ($\gtrsim 10^{53}$ erg/s) and $L_{\bar{\nu}_e}$ ($\gtrsim L_{\nu_e}$) denote the luminosity of ν_e and $\bar{\nu}_e$, respectively. Note that this enhancement of Y_e is not seen for the case in which a black hole is formed soon after the merger because of the absence of the strong neutrino source (compare the upper panels of Figs. 1 and 2).

- (iii) For the SFHo models, the dynamical ejecta mass is $\sim 0.01 M_\odot$ irrespective of the mass ratio (see Table II). The electron fraction is distributed for a wide range between 0.05 and 0.5 [40,41] (see the lower panels of Fig. 1), also irrespective of the mass

ratio. In such ejecta, an appreciable fraction of lanthanide elements should be synthesized [22, 49–51], significantly enhancing the opacity. For this EOS, the dynamical mass ejection occurs in a quasi-isotropic manner because not only the tidal effect but also the shock heating play an important role for ejecting matter (see the lower left panel of Fig. 1). Nevertheless, the matter is ejected primarily along the binary orbital plane, and ejecta in the polar direction have a minor fraction, because of the strong tidal effect during the merger and the presence of angular momentum. The ejecta near the binary orbital plane are always neutron rich with $Y_e \leq 0.25$ (see the lower panels of Fig. 1), although the ejecta in the polar region are less neutron rich.

- (iv) For the DD2 models, the dynamical ejecta mass depends strongly on the mass ratio; for $q = 1$, it is $0.002 M_\odot$, while for $q = 0.86$, it increases to $0.005 M_\odot$. The electron fraction is again widely distributed for a range between 0.05 and 0.5 [40,41] (see also the lower panels of Fig. 2) irrespective of the mass ratio. For this EOS, the matter is ejected

primarily toward the direction of the binary orbital plane because the tidal effect during the merger plays a dominant role for the mass ejection. As in the SFHo case, the ejecta in the binary orbital plane are neutron rich with $Y_e \leq 0.25$, in particular for the highly asymmetric-mass binaries. On the other hand, the ejecta in the polar region are less neutron rich with $Y_e \gtrsim 0.25$ (see the lower-right panel of Fig. 2).

- (v) The average velocity of the dynamical ejecta is $0.15\text{--}0.25c$ depending on the EOS and mass ratio. For the SFHo case, the average velocity is by 20%–30% larger than that for the DD2 case for a given value of mass because, for this EOS, the neutron-star radius is small, and hence the shock heating effect during merger enhances the kinetic energy of the ejecta.

In the above summary, the points worth noting are as follows:

- (I) No models predict the mass of the dynamical ejecta larger than $0.02 M_\odot$. This implies that if a luminous optical-IR counterpart that requires the ejecta mass of $\geq 0.02 M_\odot$ is discovered we have to consider ejecta components other than the dynamical ejecta.
- (II) Irrespective of the EOS and binary mass ratio, the electron fraction is widely distributed, and the highly neutron-rich matter is always present in the dynamical ejecta, in particular, near the binary orbital plane. Only for the direction of the rotational axis of the orbital motion ($\theta \lesssim 45^\circ$), the neutron richness is suppressed, resulting in $Y_e \gtrsim 0.25$.
- (III) Material ejected toward the polar direction ($\theta \lesssim 45^\circ$) is a minor component in terms of the mass. Although the polar ejecta have a high value of $Y_e = 0.3\text{--}0.4$, this component does not contain a sufficient amount of mass to produce a bright blue kilonova [52].

Nucleosynthesis studies (e.g., Refs. [49,50]) have shown that the presence of neutron-rich ejecta with $Y_e \lesssim 0.25$ results in producing a substantial fraction of lanthanide elements, and as a result, the opacity of the ejecta is significantly enhanced to be $\kappa \sim 10 \text{ cm}^2/\text{g}$ [19–22]. As we discuss in Sec. III A, if high-mass and low- Y_e ejecta are present along our line of sight to the source, the peak time scale of the optical light curve (in particular, for optical to near-IR light) would be long, $\gtrsim 1$ week (if the fraction of the lanthanide elements is $\gtrsim 10^{-4} M_\odot$ [51]). This effect is often referred to as the lanthanide curtain. However, the observations for GW170817 show that the optical light curve has a peak at $\lesssim 1$ day [3–13], suggesting that κ should be much smaller than $10 \text{ cm}^2/\text{g}$ for the early component of the optical-IR counterparts, and hence the contamination by lanthanide elements would be significantly suppressed at least in the outer part of the ejecta along our line of sight.

2. Remarks on neutron-star EOS

In this section, we have focused on the models employing only two representative EOS. There is a wide variety of

alternative possibilities for the neutron-star EOS. Here, we point out that for some extremely soft EOS (which still can reproduce two-solar-mass neutron stars [53]) a black hole is formed directly after the onset of merger for the total mass $m \gtrsim 2.7 M_\odot$. Such models can be constructed for EOS in which the typical stellar radius is smaller than 11 km and the maximum mass for cold spherical neutron stars is only slightly larger than $2 M_\odot$. One such example is the so-called B EOS, which is one of the piecewise polytropic EOS composed of two pieces [54,55]. For this example, a black hole is directly formed after the onset of merger for $m \geq 2.7 M_\odot$. For the case in which the mass asymmetry of the binary is not very large with this type of EOS, any torus cannot be appreciably formed surrounding the remnant black hole (e.g., Refs. [34,56]), and moreover the ejected mass cannot exceed $10^{-3} M_\odot$ (e.g., Ref. [36]). With this model, the observed electromagnetic counterparts of GW170817 cannot be described. As found for the model with the SFHo EOS and with mass $(m_1, m_2) = (1.65 M_\odot, 1.25 M_\odot)$, an appreciable mass ejection is still possible even for direct black hole formation in a case of high mass-asymmetry binaries. However, in this case, the dynamical ejecta are extremely neutrino rich so that the short peak time of the electromagnetic counterparts for GW170817 [3–13] may not be reproduced due to the lanthanide-curtain effect [51] (see the discussion in Sec. III B). These facts indicate that the optical-IR counterparts of GW170817 can be used to rule out a group of soft EOS in which the stellar radius is small (< 11 km) and the value of M_{max} is not much larger than $2 M_\odot$ (see also Ref. [57] for an independent analysis). We plan to further explore this issue by numerical-relativity simulations [58].

It should be also noted that, even for an EOS in which $R > 13$ km (e.g., H4 EOS [45]), the remnant massive neutron star could be short lived for $m \gtrsim 2.75 M_\odot$ (e.g., Refs. [35,37]) if the value of M_{max} is $\sim 2 M_\odot$. For this type of EOS, the postmerger process is likely to be similar to that for the SFHo EOS. Thus, the value of M_{max} is a key quantity for the discussion of this paper. We would like the readers to keep this point in mind.

B. Long-term evolution of merger remnants

A torus surrounding a remnant black hole or a massive neutron star with a torus could be another source for the mass ejection because the remnant torus and remnant massive neutron star are differentially rotating, and hence MHD/viscous effects induce angular momentum transport and viscous heating, which could drive long-term mass ejection, the so-called viscosity-driven mass ejection [59–63]. However, in the previous simulations [59,61–63], basically, black holes were considered as the central object. For some studies, massive neutron stars were considered as the central object, and the importance of the neutrino irradiation was qualitatively pointed out [46,60,64]. However, their treatment

for remnant massive neutron stars was rather artificial, and thus their results are not very conclusive.

Recently, we performed shear-viscous-radiation hydrodynamics simulations in general relativity for a merger remnant [65] that is obtained from one of the numerical-relativity simulations summarized in Sec. II A. Specifically, we performed simulations for the remnant of the model with the DD2 EOS and $m_1 = m_2 = 1.35 M_\odot$. We evolved both the massive neutron star and torus in a self-consistent manner. We first summarize the general properties of mass ejection for this model.

1. Evolution of massive neutron star–torus system

For our shear viscous hydrodynamics simulations [65,66], we have to give the shear viscous coefficient ν . Using the α -viscous prescription [67,68], we set it as

$$\nu = \alpha_{\text{vis}} H c_s, \quad (2.2)$$

where α_{vis} is the so-called dimensionless α parameter, H is the maximum scale height of the systems, and c_s is the sound speed. Since we are interested in the evolution of the remnant massive neutron star and the torus surrounding it, we set $H = 10$ km. We employed $\alpha_{\text{vis}} = 0.01, 0.02,$ and 0.04 following the finding in the latest high-resolution MHD simulations for accretion disks (e.g., Refs. [69–71]). Our latest high-resolution MHD simulation [72] also shows that, at least for an outer region of the remnant massive neutron star and torus, α_{vis} is likely to be enhanced to ~ 0.02 . We note that a strong turbulent state is likely to be realized in the merger remnants, because at the onset of merger, the Kelvin-Helmholtz instability and subsequent quick winding of the magnetic fields could significantly amplify the magnetic-field strength inside the remnant massive neutron star to $\gtrsim 10^{16}$ G, and as a result, MHD turbulence is likely to be induced for the remnant [72–75].

For the viscous evolution of a remnant massive neutron star surrounded by a torus, there are two mechanisms for the mass ejection [65]. In the short-term evolution with the duration in a few tens of milliseconds, the differential rotation of the remnant massive neutron star becomes the engine for the mass ejection. In the presence of viscosity, this differentially rotating state is changed to a rigidly rotating state in the viscous time scale of

$$\frac{R_{\text{eq}}^2}{\nu} \approx 23 \text{ ms} \left(\frac{\alpha_{\text{vis}}}{0.01} \right)^{-1} \left(\frac{c_s}{c/3} \right)^{-1} \left(\frac{R_{\text{eq}}}{15 \text{ km}} \right)^2 \left(\frac{H}{10 \text{ km}} \right)^{-1}, \quad (2.3)$$

where R_{eq} denotes the equatorial radius of the massive neutron star. During this transition, the density and pressure profiles are changed on the short time scale, and associated with this, strong density waves and resulting shock waves

are generated and propagate outward. Subsequently, spending a few tens of milliseconds, these shock waves sweep matter surrounding the central massive neutron star, including the torus and atmosphere around it, and provide energy to them. As a result, the matter in the outer region of the torus is ejected in a quasi-isotropic manner [65] ($\theta \gtrsim 30^\circ$; see the upper panels of Fig. 3). We refer to this mass ejection process as “early viscosity-driven mass ejection.” In our numerical experiments, the mass of this ejection is $\approx 0.01(\alpha_{\text{vis}}/0.02) M_\odot$ for $0.01 \leq \alpha_{\text{vis}} \leq 0.04$ for the case of a torus of mass $\sim 0.2 M_\odot$. This implies that if a significantly strong turbulent state is achieved in the remnant massive neutron star and the viscous parameter is effectively enhanced to be $\gtrsim 0.04$ significant mass $> 0.02 M_\odot$ would be ejected. Thus, the ejecta mass in this mechanism could be ~ 10 times as large as the dynamical ejecta mass for the DD2 model of nearly equal-mass binaries [40,41].

In this early viscosity-driven mass ejection, matter in the outer region of the torus is primarily ejected. As already pointed out in Sec. II A (see the upper panels of Fig. 2), the electron fraction for the outer part of the torus surrounding the remnant massive neutron star is fairly high as $Y_e \gtrsim 0.25$. Thus, the electron fraction for this ejecta component is typically 0.2–0.5, irrespective of α_{vis} [65] (see the upper right panel of Fig. 3). That is, mildly neutron-rich matter is ejected in contrast to the case of dynamical mass ejection. In particular, for the polar components with $\theta \lesssim 45^\circ$, Y_e is always larger than 0.3; see the upper panels of Fig. 3. Such ejecta can escape from the nucleosynthesis of an appreciable amount of lanthanide elements [65]; i.e., the opacity is not enhanced. Although the efficient heating source may not be produced from the components of $Y_e \gtrsim 0.35$ (see Fig. 5 of Ref. [50]), the fraction of such a component is minor for this mass ejection mechanism. The typical ejecta velocity for this component is ~ 0.15 – $0.20c$ depending weakly on the value of α_{vis} .

For the longer-term mass ejection with $t \gtrsim 100$ ms (up to ~ 10 s), the viscous effects on the torus surrounding the central massive neutron star play an important role [59–63]. Broadly speaking, there are two mechanisms for the mass ejection: one is viscosity-driven mass ejection with neutrino irradiation, and the other is late-time viscosity-driven mass ejection. Up to ~ 1 s (i.e., for $100 \text{ ms} \lesssim t \lesssim 1 \text{ s}$), matter ejected from the inner region of the torus accounts for an appreciable fraction. Because of the strong neutrino heating effects near the massive neutron star, in particular, in the vicinity of its polar region, the mass ejection in the vicinity of the rotational axis ($\theta \lesssim 30^\circ$) is activated; see the middle panels of Fig. 3. We refer to this mass ejection as “viscosity-driven mass ejection with neutrino irradiation.” For this component, the mass ejection rate is $\sim 10^{-3} M_\odot/\text{s}$, and the typical velocity is $\sim 0.15c$, depending weakly on the values of α_{vis} . The neutron richness of this ejecta

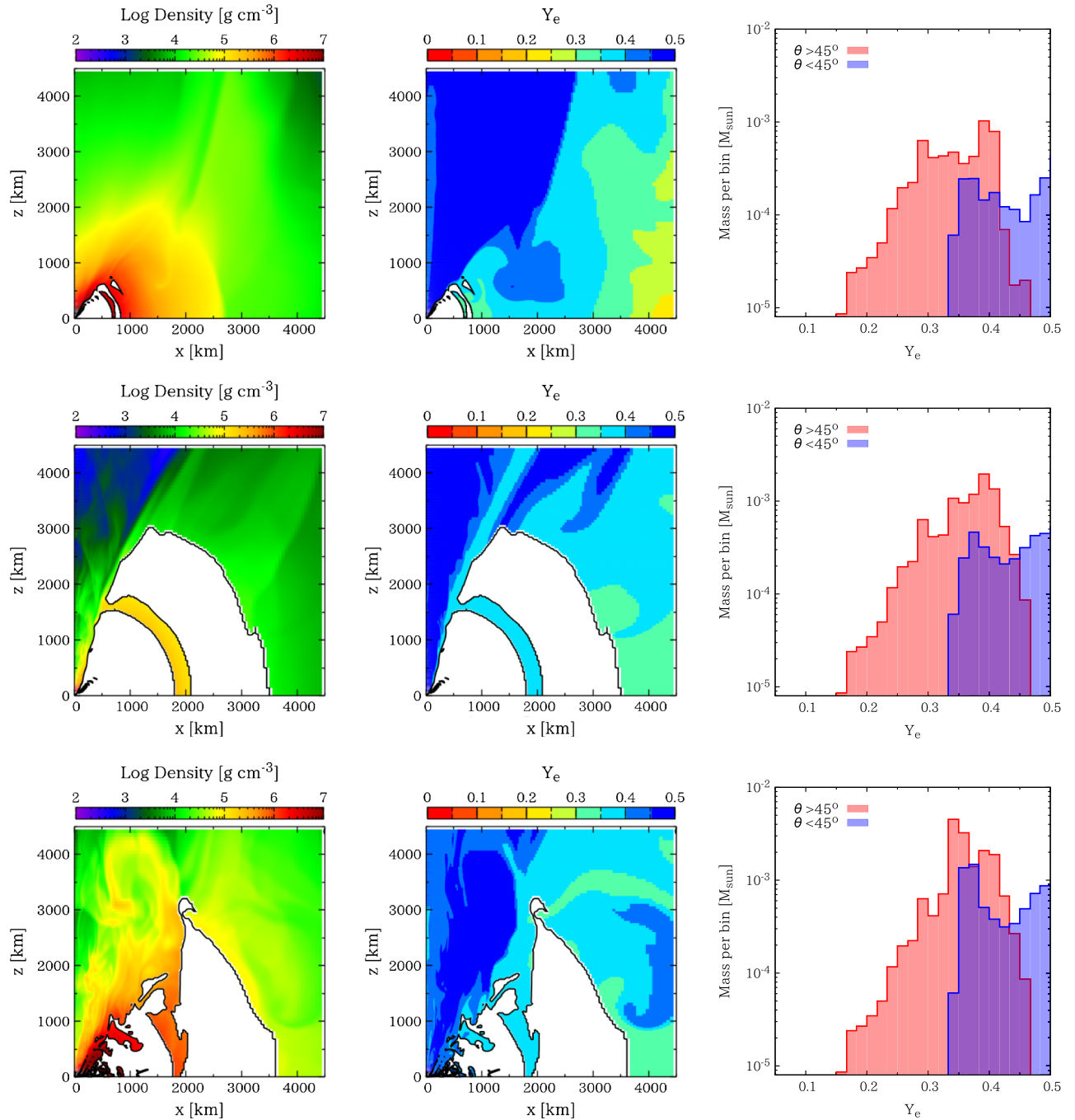


FIG. 3. The upper panels: The profiles of the rest-mass density (left) and electron fraction (middle) for the early viscosity-driven ejecta component at $t = 100$ ms after the evolution of the massive neutron star–torus system. The white region indicates that no ejecta component is present in the inner region. The right panel shows the mass histogram of the accumulated ejecta component as a function of Y_e for the regions of $z > x$ ($\theta < 45^\circ$) and $z < x$ ($\theta > 45^\circ$). The middle panels: The same as the upper panels but at $t = 500$ ms after the evolution of the system at which only the viscosity-driven ejecta from the torus with neutrino irradiation is dominant in the computational region. The bottom panels: The same as the upper panels but at $t = 1500$ ms after the evolution of the system at which the late-time viscosity-driven ejecta from the torus are driven, increasing the ejecta of $0.3 \lesssim Y_e \lesssim 0.4$. For all the panels, the results with $\alpha_{\text{vis}} = 0.04$ for the DD2 model are shown.

component is not very high with $Y_e \gtrsim 0.35$ irrespective of α_{vis} because of the neutrino irradiation from the massive neutron star (e.g., Refs. [40,46]). This indicates that this ejecta component would be free from lanthanide elements

[22,49,65], and hence the opacity for this component would be small, $\kappa \sim 0.1 \text{ cm}^2/\text{g}$. However, this ejecta component would not be a strong heating source because heavy r -process elements (that are the major heating sources) are

not synthesized from the ejecta of $Y_e \gtrsim 0.35$ [50,65].¹ This type of the mass ejection process continues as long as the massive neutron star (and torus) is present.

Our simulations for $\alpha_{\text{vis}} = 0.02$ and 0.04 were performed for a long time scale 2–3 s [65], and they show that the longer-term mass ejection from the viscosity-driven expanding torus occurs for $t \gtrsim 1$ s after the merger, but in a manner different from the viscosity-driven mass ejection with neutrino irradiation; in this late-time mass ejection mechanism, the matter is ejected primarily toward the equatorial-plane direction ($\theta \gtrsim 30^\circ$; see the bottom panels of Fig. 3). We refer to this long-term mass ejection as “late-time viscosity-driven mass ejection from torus.” The mass ejection rate for this ejection is typically $\sim 10^{-2} M_\odot/\text{s}$, depending weakly on the value of α_{vis} , and it is enhanced earlier for the larger values of α_{vis} ; this mass ejection is initially suppressed by the presence of the fall-back material that comes from the failed dynamical ejecta component, but after the density of the fall-back material decreases, the mass ejection sets in [65]. For the larger values of α_{vis} , the early viscosity-driven ejection helps to blow off a large fraction of the fall-back material, and hence this late-time viscosity-driven mass ejection sets in earlier and in a higher ejection rate. Since the mass ejection continues for seconds, the total ejecta mass in this mechanism can be appreciably larger than $10^{-2} M_\odot$ (i.e., comparable to the torus mass) for large values of $\alpha_{\text{vis}} \gtrsim 0.02$.

This late-time viscosity-driven mass ejection from the torus has been already discovered by previous works [59,60,62], and the mechanism is summarized as follows. For the late phase of the evolution of the torus $\gtrsim 1$ s, neutrino cooling becomes inefficient in the outer part of the torus with $r \gtrsim 1000$ km because its temperature decreases to $\lesssim 1$ MeV. Then, the outer part of the torus expands by the viscous heating and viscous angular momentum transport without appreciable cooling by neutrinos, primarily toward the direction of the equatorial plane ($\theta \gtrsim 45^\circ$). A part of the torus component of mass of order $10^{-2} M_\odot$ is subsequently ejected from the system spending ~ 10 s. For this component, the typical velocity is low, $\sim 0.05c$, because the mass ejection occurs far from the central object (i.e., the typical velocity scale should be low).

References [59,62,63] focus on the case in which the central object is a black hole and show that the value of Y_e for this ejecta component is unlikely to be very high for this case (see the next subsection). However, in the presence of a massive neutron star that is the strong neutrino emitter, the value of Y_e is relatively high with 0.3–0.4 (compare

¹Reference [50] shows that the heating rate of dynamical ejecta with $Y_e \gtrsim 0.35$ is suppressed by a factor of 2–3 at a few days. Note that, however, the heating rate of the first r -process peak depends sensitively on the abundance pattern. Different values of the expansion time scale and entropy would result in higher heating rates [76].

histograms in the middle and bottom panels of Fig. 3), implying that the value of κ is $\ll 10$ cm²/g. Although the low velocity may prevent the ejecta from shining in the early time of $t \lesssim$ a few days, the low value of κ may compensate this property (see Sec. III A). Since the electron fraction is not very high for this ejecta component in the presence of a massive neutron star, only relatively light r -process elements are likely to be synthesized. This suggests that the heating rate by the radioactive decay is slightly lower than that by the heavier r -process elements (see Fig. 5 of Ref. [50]).

For the early and long-term viscosity-driven ejecta, the typical velocity is smaller than $0.2c$ [65]. Thus, the velocity is slightly lower than that for the dynamical ejecta. This implies that the dynamical ejecta could not be caught up by most part of the viscosity-driven ejecta. A large fraction of the viscosity-driven ejecta would be hidden by the dynamical ejecta, if we observe the merger event from the direction of the binary orbital plane. However, for the GW170817 event, the observer is likely to be located in a polar region [1], and all the ejecta components could be observed (see Sec. III).

To summarize, we find that the total ejecta mass could be $\gtrsim 0.03 M_\odot$ for a reasonable value of $\alpha_{\text{vis}} \gtrsim 0.02$ and the electron fraction for the ejecta is mildly neutron rich in the presence of a massive neutron star; Y_e is distributed between 0.2 and 0.5, and a major fraction of the ejecta has a value of Y_e larger than 0.25. In particular, for the long-term viscosity-driven ejecta component, Y_e is likely to be always larger than ~ 0.3 . Thus, in these ejecta components, the amount of lanthanide elements should be quite small because for their nucleosynthesis a sufficiently low value of $Y_e \lesssim 0.25$ is required [22,49]. (See also Table III for a summary for mass ejection mechanisms.)

In our study, we employ a model resulting from the merger of an equal-mass binary neutron star as an initial condition. In this model, the torus mass is $\sim 0.2 M_\odot$. In the presence of asymmetry in the mass of binaries, the torus mass would be slightly larger, $\sim 0.3 M_\odot$ (see Table II). For such cases, the ejecta mass may be larger than the value estimated here. Studies for such models are left for the future. We also note that for the DD2 EOS the lifetime of the massive neutron star is quite long $\gg 1$ s. For the EOS in which the value of M_{max} is not as high as that for the DD2 EOS, the massive neutron star could collapse to a black hole within $\lesssim 1$ s. Even for such EOS, the viscosity-driven mass ejection from the torus should continue after the black-hole formation, but because of shorter neutrino-irradiation time, the value of Y_e is likely to be smaller than 0.3 in this scenario, as indicated in Ref. [60]. Studies for this case are also left for the future.

2. Evolution of black hole–torus system

To date, no detailed simulation for the evolution of black hole–torus systems incorporating both general relativistic

TABLE III. Summary of mass ejection mechanisms. The table shows the ejection type, ejecta mass, typical velocity, electron fraction, major direction of the mass ejection, and ejection duration summarized for the SFHo and DD2 models. t_ν and t denote the duration of the neutrino emission and the time after the onset of merger, respectively. We note that for the EOS in which the value of M_{max} is not as high as that for the DD2 EOS the massive neutron star could collapse to a black hole within $\lesssim 1$ s. Even for such EOS, the viscosity-driven mass ejection from the torus should continue after the black hole formation, but because of shorter neutrino-irradiation time, the value of Y_e is likely to be smaller than 0.3.

| SFHo model | | | | | |
|---|--|-------------------------|----------|----------------------------|------------------------------|
| Type of ejecta | Mass (M_\odot) | \bar{v}_{ej}/c | Y_e | Direction | Duration |
| Dynamical ejecta | $\sim 10^{-2}$ | ~ 0.2 | 0.05–0.5 | $\theta \gtrsim 45^\circ$ | $t \lesssim 10$ ms |
| Viscosity-driven ejecta from torus | $(1-2) \times 10^{-2}$ | 0.01–0.1 | 0.1–0.5 | $\theta \gtrsim 45^\circ$ | $t \sim 1-10$ s |
| DD2 model | | | | | |
| Type of ejecta | Mass (M_\odot) | \bar{v}_{ej}/c | Y_e | Direction | Duration |
| Dynamical ejecta | $O(10^{-3})$ | ~ 0.2 | 0.05–0.5 | $\theta \gtrsim 45^\circ$ | $t \lesssim 10$ ms |
| Early viscosity-driven ejecta | $\sim 10^{-2}(\alpha_{\text{vis}}/0.02)$ | 0.15–0.2 | 0.2–0.5 | $\theta \gtrsim 30^\circ$ | $t \lesssim 100$ ms |
| Viscosity-driven ejecta with neutrino irradiation | $t_\nu \times 10^{-3}/\text{s}$ | ~ 0.15 | 0.35–0.5 | $\theta \lesssim 30^\circ$ | $t \lesssim t_\nu \sim 10$ s |
| Late-time viscosity-driven ejecta from torus | $> 10^{-2}$ | ~ 0.05 | 0.3–0.4 | $\theta \gtrsim 30^\circ$ | $t \sim 1-10$ s |

gravity and neutrino heating together has been performed. The simulations for this system have been performed employing either viscous hydrodynamics in a pseudo-Newtonian gravitational field with neutrino heating and cooling [59–62] or general relativistic magnetohydrodynamics in a Kerr black hole background with no neutrino heating [63]. We summarize here the results obtained from these simulations.

Simulations for spinning black hole–torus systems [59–63] with a high black hole spin of ~ 0.8 indicate that $\sim 20\%$ of the torus mass could be ejected as a wind component through the long-term viscous process in the torus. As already mentioned in the previous subsection, Sec. II B 1, this viscosity-driven ejection takes place for $t \gtrsim 1$ s after the temperature of the torus decreases to $\lesssim 1$ MeV. All the previous simulations suggest that these viscosity-driven ejecta are fairly neutron rich with $Y_e = 0.1-0.5$ and with the peak at $Y_e = 0.2-0.3$ [59–63]. This indicates that the opacity for this component is likely to be as high as that for the dynamical ejecta component because of the nucleosynthesis of lanthanide elements. Also shown is that the velocity of this ejecta component is relatively low as $0.01-0.1c$, with the typical velocity $\sim 0.05c$, because the mass ejection from the torus occurs in a region distant from the central region. Thus, this component may not be well suited for describing the early shining of GW170817 [see Eq. (3.1)].

The mass ejection in this viscous process primarily proceeds in the direction of the equatorial plane; only a minor fraction of the mass is ejected toward the polar direction. The recent MHD simulation in general relativity [63] indicates that the ejecta properties are slightly modified by the MHD effect. One effect observed in the MHD simulation is the increase of the fraction of the polar ejecta component. However, the equatorial ejecta component is

still dominant over the polar one even in the MHD simulation, and, overall, the ejecta are always neutron rich.

One of the concerns for these simulations is that initial conditions might not be very realistic. The initial rotational profile was typically given by assuming a constant specific angular momentum, which is far from Keplerian and hence not very physical. In addition, the $Y_e = 0.1$ profile is initially given taking into account that the accretion torus is neutron rich because of its high density resulting in a high degeneracy of electrons. However, in reality, the outer part of the torus is likely to have a larger value of Y_e up to ~ 0.4 in the context of binary neutron-star mergers (see the upper panel of Fig. 1). For this problem, more detailed realistic simulations are awaited. However, in the following section, we discuss possible scenarios based only on our results and those reported in Refs. [59–63].

III. MODELS FOR GW170817

A. Models for macronova/kilonova

First, we summarize several approximate relations satisfied for the macronova/kilonova model [15,16]. The energy source in this model is the radioactive decay of r -process elements. As the radioactive heating rate declines monotonically with time, the observed luminosity reaches the peak, L_{peak} , on the photon diffusion time scale of the ejecta (e.g., Ref. [16]),

$$\begin{aligned}
 t_{\text{peak}} &\approx \sqrt{\frac{\xi \kappa M_{\text{ej}}}{4\pi c \bar{v}_{\text{ej}}}} \\
 &\approx 1.9 d_\xi^{1/2} \left(\frac{\kappa}{1 \text{ cm}^2/\text{g}}\right)^{1/2} \left(\frac{M_{\text{ej}}}{0.03 M_\odot}\right)^{1/2} \left(\frac{\bar{v}_{\text{ej}}}{0.2c}\right)^{-1/2},
 \end{aligned}
 \tag{3.1}$$

where ξ is a parameter associated with the degree of asphericity of the ejecta with $\xi \leq 1$, which depends on the geometry of the ejecta. We note that the asphericity of the ejecta profile can decrease ξ along our line of sight. However, the degree of the asphericity for the dynamical and viscosity-driven ejecta is $1/2 \lesssim \xi \leq 1$ (unless the binary mass asymmetry is extremely high), and hence its effect is not very significant [52]. Thus, the peak time is unlikely to be significantly different from Eq. (3.1). We note that it is possible to consider that the velocity is enhanced effectively by ξ as \bar{v}_{ej}/ξ . Thus, in the presence of the asphericity, the effectively velocity can be increased if we consider a model in the assumption of spherical symmetry. We also note that the peak luminosity and temperature can be enhanced by the asphericity effect [77,78]; these effects should be taken into account for detailed modeling.

Although the energy generation rate of beta decay in the macronova/kilonova emission is robustly described as $\propto t^{-1.3}$ for $t \gtrsim 1$ d [16,79], the thermalization efficiency of decay products in the ejecta has to be taken into account for the actual heating rate. The specific heating rate for the hypothetical abundance, in which the solar-abundance pattern is assumed to be achieved, is given approximately as (e.g., see Refs. [78,80])

$$\dot{\epsilon} \approx 1.6 \times 10^{10} \text{ erg/s/g} \left(\frac{t}{\text{day}} \right)^{-1.3}, \quad (3.2)$$

when both electrons and gamma rays are fully thermalized. Gamma rays start leaking from the ejecta at $t_{\text{in},\gamma} \approx 0.6 \text{d} (M_{\text{ej}}/0.03 M_{\odot})^{1/2} (\bar{v}_{\text{ej}}/0.2c)^{-1/2}$, where we used the inelasticity of the Compton scattering [80,81]. The thermalization of electrons starts being inefficient at $t_{\text{in},e} \approx 18 \text{d} (M_{\text{ej}}/0.03 M_{\odot})^{1/2} (\bar{v}_{\text{ej}}/0.2c)^{-3/2}$ [81]. For $t_{\text{in},\gamma} \lesssim t \lesssim t_{\text{in},e}$, the radioactive heating is dominated by electrons, and the specific heating rate is described approximately by

$$\dot{\epsilon} \approx 0.5 \times 10^{10} \text{ erg/s/g} \left(\frac{t}{\text{day}} \right)^{-1.3}. \quad (3.3)$$

In addition to beta decay, alpha decay and spontaneous fission may significantly enhance the heating rate at late times depending on the abundance of heavy nuclei $A \geq 210$. It is worth noting that the heating rate of alpha decay and fission arises, at late times, at a shallower decline rate $\propto t^{-1}$ than that of beta decay [80,81]. We also note that in the absence of heavy r -process elements (like second- and third-peak elements) the heating rate would be much lower than that shown here (see Fig. 5 of Ref. [50]).

For $t \gtrsim t_{\text{peak}}$, the total luminosity (in the hypothetical presence of heavy r elements) is given approximately by

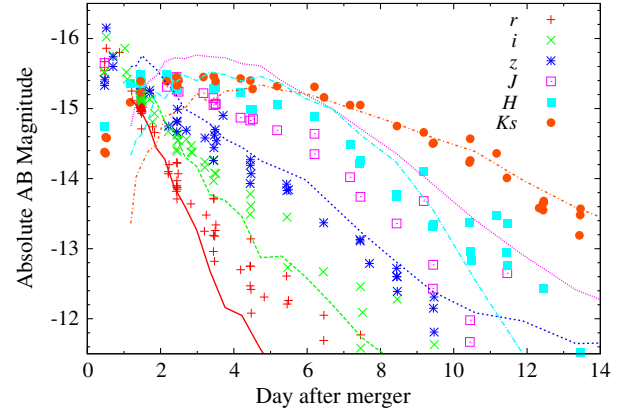


FIG. 4. Observational light curves (in terms of the data taken from Ref. [82]) and a light curve model [3] of the electromagnetic counterparts of GW170817. Plotted are the absolute AB magnitudes for the r , i , z , J , H , and K_s bands. The horizontal axis shows the day spent after merger of the binary neutron stars. Here, we assume that the distance to the source is 40 Mpc.

$$L \approx \dot{\epsilon} M_{\text{ej}}$$

$$= (0.3-1.0) \times 10^{42} \text{ erg/s} \left(\frac{M_{\text{ej}}}{0.03 M_{\odot}} \right) \left(\frac{t}{\text{day}} \right)^{-1.3}. \quad (3.4)$$

We note that in the presence of other strong energy sources, e.g., a magnetar central engine, the total luminosity may be higher than that in Eq. (3.4), but in this section, we do not consider this possibility.

Figure 4 shows observational light curves for which the data are taken from Ref. [82]. For describing the electromagnetic counterparts of GW170817 for $t \lesssim 5$ days, the following observational results give the fundamental constraints to the free parameters such as the ejecta mass, velocity, and opacity:

- (i) The peak absolute (AB) magnitude in the r , i , and z bands is ≈ -16 mag assuming that the distance to the source is 40 Mpc [the required luminosity for these bands is, broadly speaking, $(3-5) \times 10^{41}$ erg/s], and the peak luminosity is reached within ~ 1 day after the merger.
- (ii) The peak absolute magnitude in the IR bands (J , H , and K bands) is ≈ -15.5 mag (the required luminosity for these bands is approximately 10^{41} erg/s for the J band and 3×10^{40} erg/s for the K band), and this peak luminosity is reached in a week after the merger. Note that the observed spectrum is consistent broadly with the blackbody one with decreasing temperature (but see Ref. [83] for detailed comparisons), and hence the evolution of the luminosity is consistent with the macronova/kilonova model.

The early peak time for these observational results suggests that the opacity cannot be as large as $\kappa = 10 \text{ cm}^2/\text{g}$ even for $\bar{v}_{\text{ej}} \sim 0.2c$ [see Eq. (3.1)]. The high

peak luminosity also suggests that the ejecta mass should be appreciably larger than $0.01 M_{\odot}$ [see Eq. (3.4)]. The constraint, $\kappa \ll 10 \text{ cm}^2/\text{g}$, implies that the electromagnetic counterpart should not contain a large amount of lanthanide elements at least along our line of sight in the early time (for a few days after the onset of merger). This strongly suggests that the ejecta would be composed not only of dynamical ejecta but also of other components like viscosity-driven ejection components because the dynamical ejecta primarily synthesize heavy r -process elements including lanthanide elements. Also the high luminosity (i.e., high ejecta mass $> 0.01 M_{\odot}$) suggests that the ejecta would not be composed only of dynamical ejecta.

In the late phase of the electromagnetic counterparts of GW170817 with $t \gtrsim 5$ days, a significantly reddening feature is found (e.g., Refs. [6,10,84]). For describing this component, the opacity should be high $\kappa \sim 10 \text{ cm}^2/\text{g}$, and hence an appreciable amount of the lanthanide synthesis is required. This component is likely to be supplied from the dynamical ejecta and viscosity-driven components obscured by the dynamical ejecta.

The solid curves of Fig. 4 denote a light curve model [3] for the electromagnetic counterparts of GW170817. This model assumes that the spherical ejecta expand in a homologous manner with the average velocity $0.1c$ and with the mass $M_{\text{ej}} = 0.03 M_{\odot}$. In this example, the opacity is determined for a hypothetical abundance of r -process elements synthesized from the ejecta of $Y_e = 0.25$ [22] and results approximately in $\kappa \sim 1 \text{ cm}^2/\text{g}$. This model approximately captures the features for the observed event. We note that for a model in which $M_{\text{ej}} = 0.03 M_{\odot}$ and $\kappa = 10 \text{ cm}^2/\text{g}$ the i -band luminosity at $t = 1$ day is only ≈ -15 mag, and moreover the peak time for the H band is delayed significantly to $t_{\text{peak}} \gtrsim 5$ days [22]. These results suggest that the low value of κ is one of the keys for interpreting the observational results of GW170817.

Paying particular attention to the two constraints (i) and (ii), we explore here the following two scenarios for interpreting the GW170817 event: one scenario is based on the numerical results with the SFHo EOS, and the other is based on the results with the DD2 EOS. For the given constraint to the total mass of the binary neutron stars of GW170817, $m \geq 2.73 M_{\odot}$, in the former, the remnant is a spinning black hole surrounded by a torus, and in the latter, it is a long-lived massive neutron star surrounded by a torus. In the following subsections, we finally conclude that (I) the current numerical-relativity simulations do not support the SFHo model in which a black hole is formed in a short time scale after the onset of merger, and hence long-term strong sources for the neutrino irradiation may be absent in the merger remnant (because of the same reason [85,86], the black hole–neutron star model for GW170817 is likely to be rejected by the observation of the electromagnetic counterparts), and (II) the presence of a long-lived remnant massive neutron star found in the DD2

model, which is a long-term strong emitter of neutrinos and is suitable for increasing the electron fraction of the ejecta, is favorable for interpreting the observational results of GW170817.

For help in understanding each model, in Table III, we summarize the type of the ejecta and properties of each ejecta component for the SFHo and DD2 models separately.

B. Scenario for the soft EOS

First, we describe the scenario based on the numerical-relativity results for the SFHo EOS as a model that is not well suited for interpreting the observations for the electromagnetic counterparts of GW170817. As shown in Sec. II A, in this EOS model, the merger with $m = 2.7\text{--}2.8 M_{\odot}$ results in temporal formation of a hypermassive neutron star, and it collapses, in $\lesssim 10$ ms after its formation, to a spinning black hole of dimensionless spin ~ 0.7 surrounded by a torus of mass $\sim 0.1 M_{\odot}$. Because the lifetime of the hypermassive neutron star is shorter for the higher total mass of the system, we assume here that the lifetime would be $\lesssim 5$ ms, taking into account the total mass of GW170817, $m \gtrsim 2.73 M_{\odot}$ [i.e., we assume that the lifetime would be shorter than the viscous time scale in the hypermassive neutron star, written in Eq. (2.3)]. In this model, the mass of the dynamical ejecta is $\sim 0.01 M_{\odot}$, and these dynamical ejecta always contain a substantial fraction of neutron-rich elements with $Y_e \lesssim 0.2$ irrespective of the total mass and mass ratio. Thus, the opacity of the dynamical ejecta is high as $\kappa \sim 10 \text{ cm}^2/\text{g}$ [19–22] due to the existence of an appreciable amount of lanthanide elements [22,49]. The dynamical ejecta have a quasi-isotropic shell structure (see Fig. 5).

For this model, the remnant black hole is surrounded by a torus of mass $0.05\text{--}0.1 M_{\odot}$. Simulations for spinning black hole–torus systems [59–63] indicate that $\sim 20\%$ of the torus mass could be ejected as a viscosity-driven component through the long-term viscous process in the torus. This suggests that by the viscous process matter with mass of $\sim 0.01\text{--}0.02 M_{\odot}$ could be ejected. However, these previous simulations suggest that this viscous component is fairly neutron rich of a wide distribution of $Y_e = 0.1\text{--}0.5$ with the peak at $Y_e = 0.2\text{--}0.3$. From such ejecta, an appreciable amount of lanthanide elements should be synthesized [22,49]. This indicates that the opacity for this component is likely to be as high as that for the dynamical ejecta component. Also shown is that the mass ejection in this viscous process primarily proceeds to the direction of the equatorial plane (not to the polar direction). The typical velocity of this ejecta component is lower than that for the dynamical ejecta, and in addition, its morphology is similar to that of the dynamical ejecta (for which the mass ejection occurs also primarily in the direction of the binary orbital plane). All these facts suggest that the time scale to reach the peak luminosity is likely to be much

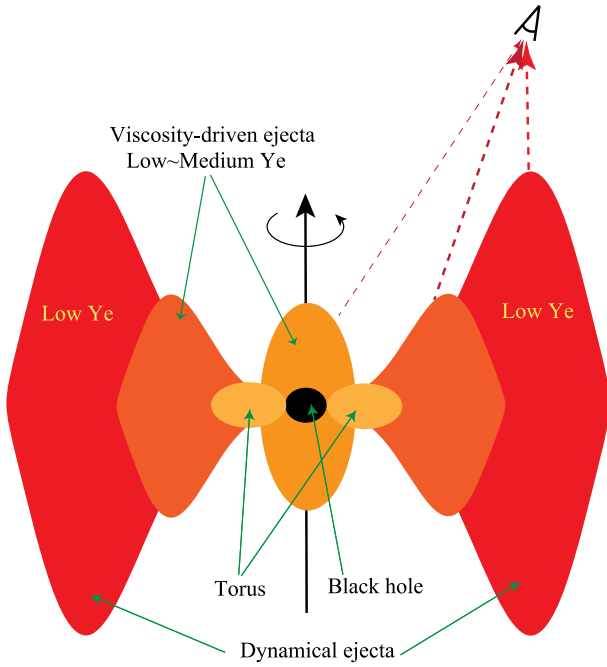


FIG. 5. Schematic picture of the ejecta profile for the case of a soft EOS in which a black hole is formed in ~ 10 ms after the onset of merger. The largest anisotropic-shell component (red color) denotes the dynamical ejecta. The smaller anisotropic-shell (red) and polar components (ocher) denote the viscous and MHD ejecta from the torus, respectively. “Low Y_e ” implies that it contains neutron-rich matter with $Y_e \lesssim 0.2$, which synthesizes an appreciable amount of lanthanide elements and contributes to enhancing the opacity to $\kappa \sim 10$ cm²/g. The polar component could have ejecta of $Y_e = 0.3$ – 0.4 , but it is a minor component in mass. The black filled circle and neighboring (orange) ellipsoids in the central region denote a spinning black hole and accretion torus surrounding the black hole, respectively. Since the opacity is entirely high for all the major ejecta components, it is difficult to describe the observational results (in particular, early peak time) for the electromagnetic counterparts of GW170817 by this model.

longer than 1 day due to the high opacity and $\bar{v}_{ej} \leq 0.25c$ even for $\xi \sim 1/2$ [see Eq. (3.1)]; this model is not suitable for reproducing the optical-IR counterparts for GW170817. We speculate that this conclusion may be universal for any EOS model in which a long-lived massive neutron star is not formed as the merger remnant. For examining this speculation, we need to perform more simulations employing different EOS.

If significant viscosity-driven mass ejection could occur in the polar direction with high velocity and with moderate neutron richness as $Y_e \gtrsim 0.25$, this model could be viable. Such ejection may be possible if significant neutrino heating occurs from the inner edge of the torus around a spinning black hole. Indeed, general relativistic simulations of Ref. [87] (with no neutrino heating) suggest that strong neutrino emission with a luminosity of appreciably higher than 10^{52} erg/s may be possible from a torus of

mass $\gtrsim 0.1 M_\odot$ surrounding a spinning black hole of dimensionless spin 0.75. This possibility deserves more detailed exploration. For this purpose, we need a detailed numerical work incorporating neutrino heating and general relativity for the evolution of the merger remnant.

C. Scenario for the stiff EOS

As shown in Sec. II A, in the stiff EOS model like DD2, the merger for $m = 2.7$ – $2.8 M_\odot$ results in the formation of a long-lived massive neutron star, which is differentially rotating at its formation. The remnant massive neutron star is surrounded by a dense torus of mass ~ 0.2 – $0.3 M_\odot$.

For this model, the mass of the dynamical ejecta is of order $10^{-3} M_\odot$. These ejecta contain a sufficient fraction of the low- Y_e component, and hence a significant amount of lanthanide elements are synthesized, resulting in a high opacity, $\kappa \sim 10$ cm²/g. The dynamical ejecta have an anisotropic-shell structure in this EOS (see Fig. 6). The typical ejecta velocity is $\bar{v}_{ej} \sim 0.2c$ or slightly slower.

Because the remnant massive neutron star is initially differentially rotating, the subsequent mass ejection is likely to be induced by the viscous effects (i.e., early viscosity-driven mass ejection). As described in Sec. II B, the degree of differential rotation of the remnant neutron star decreases with time, and it approaches a rigidly rotating state on a time scale of ~ 10 – 20 ms with a reasonable value of α_{vis} [see Eq. (2.3)]. During the transition of this rotating state, matter is likely to be ejected. This mass ejection occurs in a fairly anisotropic manner, and the typical ejecta velocity is $\bar{v}_{ej} = 0.15$ – $0.20c$, i.e., slightly smaller than that of the dynamical ejecta. The neutron richness of this ejecta component is mildly high, i.e., $Y_e \approx 0.2$ – 0.5 [65]. What is nice in this ejection is that for the high latitude ($\theta \lesssim 45^\circ$) the fraction of neutron-rich matter is small (see Figs. 3 and 6). If the turbulent state of the remnant massive star is sufficiently enhanced and the resulting effective viscous parameter is sufficiently large as $\alpha_{vis} \gtrsim 0.02$, the ejecta mass in this mechanism could be $> 0.01 M_\odot$.

Since the torus surrounding the central massive neutron star is also differentially rotating, the viscosity-driven mass ejection from the torus occurs for a long time scale of ~ 1 – 10 s following the early viscosity-driven ejection. For 100 ms $\lesssim t \lesssim 1$ s, this mass ejection proceeds primarily toward the polar direction because of the strong neutrino heating near the remnant massive neutron star (viscosity-driven mass ejection with neutrino irradiation) [65]. The typical ejecta velocity is $\bar{v}_{ej} = 0.1$ – $0.2c$ depending weakly on the value of α_{vis} . The neutron richness of this ejecta component is not high, $Y_e \gtrsim 0.35$, because of the strong neutrino irradiation from the remnant neutron star, and hence the heating rate is sensitive to the elemental abundance pattern, as already mentioned in Sec. II B.

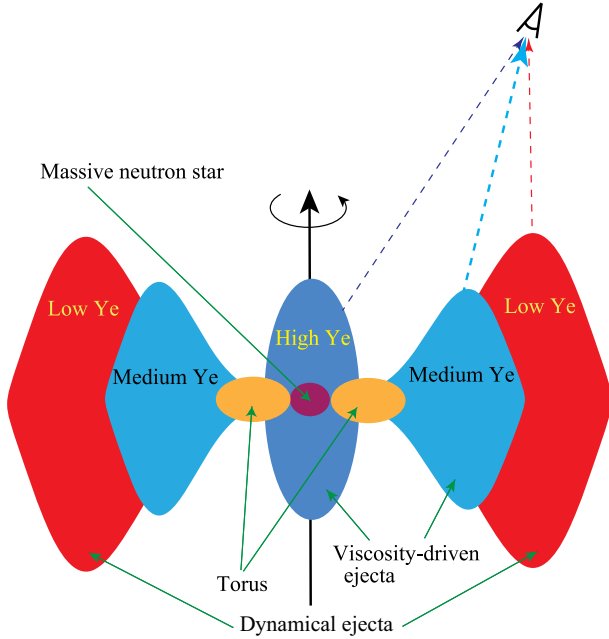


FIG. 6. Schematic picture of the ejecta profile for the case of a stiff EOS in which a long-lived massive neutron star is formed as a remnant. The largest anisotropic-shell component (red color) denotes the neutron-rich dynamical ejecta. The smaller anisotropic-shell component (blue color) denotes the early viscosity-driven ejecta and long-term viscosity-driven ejecta from the torus. The polar spheroid component (dark blue color) denotes the viscosity-driven ejecta from the torus influenced by neutrino irradiation from the massive neutron star. Low Y_e implies that it contains neutron-rich matter with $Y_e \lesssim 0.2$, which contributes to enhancing the opacity through the nucleosynthesis of lanthanide elements. “Medium Y_e ” and “high Y_e ” imply that it does not contain such neutron-rich matter because $Y_e \gtrsim 0.25$ and $Y_e \gtrsim 0.35$, respectively. The filled (purple) circle and neighboring small (orange) ellipsoids in the central region denote a massive neutron star and accretion torus surrounding it. We note that the low- Y_e component has a high average expansion velocity of $\bar{v}_{ej} \sim 0.2c$, while the medium and high components have slower velocity, $0.1\text{--}0.2c$. Note that the gravitational-wave observation indicates that we observe the merger remnant of GW170817 along the direction of $\theta \leq 28^\circ$ from the rotation axis.

In the later phase of the viscosity-driven mass ejection ($t > 1$ s), the mass is primarily ejected in a weakly anisotropic manner with the average mass ejection rate of $10^{-2} M_\odot/s$ and with low velocity $\sim 0.05c$ (late-time viscosity-driven mass ejection from the torus). For this component, the value of Y_e is $0.3\text{--}0.4$. (If the lifetime of the massive neutron star is shorter than ~ 1 s, the value of Y_e may be smaller than 0.3 .) Thus, we may expect a weak lanthanide contamination and the presence of a relatively strong heating source (not as strong as by the heavier r -process elements [50]). This mass ejection from the expanding torus is likely to continue for ~ 10 s as found in Ref. [60], and the ejecta mass also could be of order $0.01 M_\odot$.

All these discussions (based mainly on our numerical-relativity simulations) suggest that in this model the mass of the mildly neutron-rich viscosity-driven ejecta with the velocity $0.05\text{--}0.15c$ could be $\gtrsim 0.03 M_\odot$ in total for $\alpha_{vis} \gtrsim 0.02$. Since most of these viscosity-driven ejecta are not highly neutron rich with $Y_e \gtrsim 0.25$, and thus the nucleosynthesis of lanthanide elements would be suppressed, their opacity is likely to be $\kappa \lesssim 1 \text{ cm}^2/\text{g}$ [22,49,51]. In particular, for the ejected matter located for the high latitude ($\theta \lesssim 45^\circ$), Y_e is always high (see Figs. 3 and 6). This indicates that if an observer is not located near the binary orbital plane the effect of the lanthanide curtain provided by the dynamical ejecta could be avoided. Then, if the mass of the viscosity-driven ejecta is sufficiently high as $\gtrsim 0.03 M_\odot$ (i.e., α_{vis} is sufficiently large $\sim 0.02\text{--}0.04$), the electromagnetic observations for GW170817 can be naturally interpreted.

One unclear point in the early viscosity-driven ejection is that we do not know whether α_{vis} is really sufficiently large $\sim 0.02\text{--}0.04$ around the central region of the remnant massive neutron star, i.e., a sufficiently strong turbulence state is realized or not there, although $\alpha_{vis} = O(0.01)$ is a reasonable magnitude for turbulent fluids; indeed, our latest high-resolution MHD simulation [72] shows that, at least for an outer region of the remnant massive neutron star and torus, α_{vis} is likely to be enhanced to ~ 0.02 . To assess the validity of this scenario, however, we need to perform a high-resolution MHD simulation for the merger and post-merger of binary neutron stars, in which several MHD instabilities such as Kelvin-Helmholtz and magnetorotational instabilities are well resolved. We note that if the initial torus mass of the merger remnant is higher (e.g., for the merger of significant binary mass asymmetry) the ejecta mass of $\gtrsim 0.03 M_\odot$ may be achieved for a smaller value of α_{vis} . Thus, the required value for α_{vis} may be smaller.

In this section, we have paid particular attention to the optical-IR counterparts in the relatively early phase of $\lesssim 5$ days. In the late phase, the effect of the dynamical mass ejection of low Y_e (i.e., of high values of κ) should be visible. The late-time reddening [6,10,84] is likely to be associated with the dynamical ejecta component in our scenario.

IV. DISCUSSION

A. Perspective for constraining the neutron-star EOS through measuring tidal deformability

In Sec. III, we proposed a model of the binary neutron-star merger suitable for interpreting the observational results for the electromagnetic signals of GW170817. Our analysis suggests that the neutron-star EOS would be stiff enough (i.e., the maximum mass for cold spherical neutron stars is large enough) to produce a long-lived massive neutron star after the merger for the total mass $m \gtrsim 2.73 M_\odot$. However, this suggestion primarily

constrains the maximum mass of cold neutron stars, not the neutron-star radius.

One of the most promising methods to narrow down the possible EOS candidates by constraining the typical radius of neutron stars is to measure the tidal deformability of neutron stars through the gravitational-wave observation of the late inspiral signals of binary neutron stars (e.g., Refs. [88–92]). For an event of $S/N \approx 30$ to LIGO O2 sensitivity (for which the sensitivity for a high-frequency band $\gtrsim 400$ Hz is not as good as for the lower band [93]), the binary dimensionless tidal deformability, Λ , would be distinguished up to $\delta\Lambda \approx 400$ at $2 - \sigma$ level by analyzing gravitational waves from binary neutron stars in close orbits [88,92]. Here, Λ is defined by

$$\Lambda = \frac{8}{13} \left[(1 + 7\eta - 31\eta^2)(\Lambda_1 + \Lambda_2) - \sqrt{1 - 4\eta(1 + 9\eta - 11\eta^2)}(\Lambda_1 - \Lambda_2) \right], \quad (4.1)$$

and Λ_1 and Λ_2 are each dimensionless tidal deformability in binaries. It is known that for a given value of the chirp mass Λ depends very weakly on mass ratio (see, e.g., the last five data in each row of Table I [94]). The gravitational-wave observation of GW170817 preliminarily suggests that Λ is smaller than ~ 800 as the 90% credible upper limit for a hypothesis that the dimensionless spin parameter of neutron stars is smaller than 0.05 [1]. Thus, the DD2 EOS is marginally acceptable, although the template employed in this preliminary analysis tends to indicate a value of Λ [92] larger than the true one. The error size for the observational result of GW170817 is consistent with the analysis of Refs. [88,92]. We note that this observational result suggests that the neutron-star radius of mass $1.35 M_\odot$ should be smaller than ~ 13 km at the 90% credible upper limit (see, e.g., Table I).

For the SFHo EOS in which the typical neutron-star radius is $R \sim 12$ km, the maximum mass of cold spherical neutron stars is $M_{\max} \approx 2.06 M_\odot$. For such a type of EOS, long-lived massive neutron stars cannot be formed after the merger for $m \gtrsim 2.7 M_\odot$. However, if M_{\max} is appreciably larger than $2 M_\odot$ for an EOS of $R \lesssim 12$ km due to significant stiffening of the EOS for the supra-nuclear-density region like in the EOS of Ref. [95] (for which $M_{\max} \approx 2.21 M_\odot$ and $R \sim 11.5$ km), a long-lived massive neutron star may be formed after the merger for $m \gtrsim 2.73 M_\odot$. The maximum mass cannot be increased arbitrarily because the sound speed has to be always smaller than the speed of light. However, detailed analyses of spherical neutron stars [96] show that the maximum mass can be as high as ~ 2.2 – $2.3 M_\odot$ even for the neutron-star radius of 11–12 km. The gravitational-wave and electromagnetic observations for GW170817 suggest that such an EOS is a candidate even if the typical radius is small.

B. Possible constraint to the neutron-star EOS through the observations of electromagnetic counterparts

A possible constraint on the neutron-star EOS is obtained from the absence of observational evidence for the existence of a rapidly rotating magnetar remnant, which can release its rotational kinetic energy,

$$T_{\text{rot}} \approx 1.1 \times 10^{53} \text{ erg} \left(\frac{M_{\text{MNS}}}{2.5 M_\odot} \right) \left(\frac{R}{15 \text{ km}} \right)^2 \left(\frac{\Omega}{7000 \text{ rad/s}} \right)^2, \quad (4.2)$$

where we used $T_{\text{rot}} = I\Omega^2/2$ and $I = 0.4M_{\text{MNS}}R^2$ [97] with I the moment of the inertia and M_{MNS} the mass of the massive neutron star. As mentioned in Sec. II B 1, the remnant massive neutron star is likely to be strongly magnetized due to several amplification processes of the magnetic-field strength during the merger [72,74,75]. If a force-free dipole magnetic field with a strong magnetic-field like in magnetars [98] is established outside the merger remnant, the system would release its rotational kinetic energy through strong magnetic dipole radiation with luminosity [68],

$$\begin{aligned} L_{\text{mag}} &\approx \frac{B_p^2 R^6 \Omega^4}{6c^3} \\ &\approx 1.7 \times 10^{50} \text{ erg/s} \left(\frac{B_p}{10^{15} \text{ G}} \right)^2 \left(\frac{R}{15 \text{ km}} \right)^6 \\ &\quad \times \left(\frac{\Omega}{7000 \text{ rad/s}} \right)^4, \end{aligned} \quad (4.3)$$

where B_p is the magnetic-field strength at the polar region, R is the typical radius, and Ω is the angular velocity of the remnant massive neutron star, respectively. Thus, the spin-down time scale of the remnant massive neutron star defined by $T_{\text{rot}}/L_{\text{mag}}$ is estimated as

$$\begin{aligned} \tau_B &\approx 650 \text{ s} \left(\frac{B_p}{10^{15} \text{ G}} \right)^{-2} \left(\frac{M_{\text{MNS}}}{2.5 M_\odot} \right) \\ &\quad \times \left(\frac{R}{15 \text{ km}} \right)^{-4} \left(\frac{\Omega}{7000 \text{ rad/s}} \right)^{-2}. \end{aligned} \quad (4.4)$$

As this spin-down process occurs on a time scale during which the ejecta are still optically thick, the remnant magnetar produces a hot bubble inside the ejecta, which accelerates the ejected matter. Thus, the rotational kinetic energy is converted to the ejecta's kinetic energy. If a substantial fraction of T_{rot} is injected into the ejecta, we expect to observe (i) the expansion velocity of $\bar{v}_{\text{ej}} \approx c$ (because $T_{\text{rot}} \gtrsim M_{\text{ej}}c^2$) and (ii) very bright radio, optical, and x-ray signals [99–101]. However, the electromagnetic observations for GW170817 did not show any evidence of these features. One possible interpretation for this is that such a strong dipole magnetic field would not be

established outside the remnant on a time scale of a month, although the magnetic field inside the massive neutron star is very strong $\gtrsim 10^{16}$ G. However, this is not very natural because there are many neutron stars of strong magnetic fields in nature [98].

Another interpretation is that the massive neutron star collapses to a black hole before a substantial fraction of the rotational kinetic energy is released. This condition is satisfied for the case in which the remnant object is a hypermassive neutron star. However, it is difficult to interpret the fast rise of the optical-IR light curves if the lifetime of the hypermassive neutron star is too short, e.g., the SFHo EOS case, as discussed in Sec. III. A more favored scenario is that the hypermassive neutron star collapses in a time scale of the neutrino cooling of ~ 10 s $\ll \tau_B$. If high-luminosity gamma rays detected by Fermi and INTEGRAL come from a black hole surrounded by a torus, the collapse to the black hole may occur at $\lesssim 1$ s. This scenario could be satisfied in the case of a stiff EOS. If this is the case, the maximum mass of the neutron star could be constrained. For instance, the gravitational mass of the remnant massive neutron star at the collapse is likely to be $\sim (2.60 \pm 0.05) M_\odot$ for the total mass of the binary for GW170817, $m = 2.73\text{--}2.78 M_\odot$, because the gravitational-wave emission (primarily during the inspiral phase), the long-term neutrino emission (in the postmerger phase), and the mass ejection reduce the mass of the system by $\sim (0.15 \pm 0.03) M_\odot$ in total (supposing that the lifetime of the hypermassive massive neutron stars is $\sim 0.5\text{--}2$ s). We suppose that at the onset of the collapse to a black hole the gravitational mass of the remnant massive neutron star in rapid rotation would be such values. Because the rapid and rigid rotation increases the maximum-allowed mass for neutron stars by $\sim 0.4 M_\odot$ [102], the expected maximum mass for cold spherical neutron stars would be $\sim 2.15\text{--}2.25 M_\odot$ (i.e., the maximum mass for the DD2 EOS is slightly larger than the required value). This is a reasonable value for typical stiff EOS (see also Ref. [103] for an independent analysis).

C. Implications of GW170817 event for r -process nucleosynthesis

Our model with the DD2 EOS shows that the total mass of ejected heavy r -process elements with mass number $A \gtrsim 90$ (i.e., the so-called second and third peak elements) would be several $\times 10^{-3} M_\odot\text{--}10^{-2} M_\odot$. In our model, such r -process elements are likely to be synthesized partly from the dynamical ejecta and primarily from the early viscosity-driven ejecta [65]. For the latter, the r -process elements only up to the second peak would be formed [65], but because the total ejected mass by this mechanism dominates over that of the dynamical ejecta, it will contribute to the majority of the total mass of r -process elements. On the other hand, the dynamical ejecta will contribute primarily to synthesis of the third-peak and

lanthanide elements because its neutron richness is quite high [40,41].

Assuming that the solar abundance [104] gives the mean values for stars in the Galactic disk, the total mass of heavy r -process elements with $A \geq 90$ in our Galaxy is approximately $5 \times 10^3 M_\odot$. These elements also indicate a uniform abundance pattern in metal-poor stars [105]. This suggests that they are synthesized in a single kind of the phenomenon. As discussed in Ref. [106], mergers of neutron-star binaries (binary neutron stars and black hole–neutron star binaries) are among the most promising candidates for the source of the r -process nucleosynthesis. Here, we assume that the binary neutron-star mergers are the dominant nucleosynthesis sources. Since GW170817 indicates that the neutron-star radius is fairly small [1] and hence tidal disruption of neutron stars by black holes becomes less likely, this may be now a reasonable assumption.

If the r -process nucleosynthesis has occurred uniformly in the history of our Galaxy, the merger rate of binary neutron stars is estimated to be

$$10^{-4} \text{ yr}^{-1} \left(\frac{M_{A \geq 90}}{5 \times 10^{-3} M_\odot} \right), \quad (4.5)$$

where $M_{A \geq 90}$ denotes the average total mass of r -process elements with $A \geq 90$ that are synthesized in one merger event. This event rate may be slightly larger than the latest estimates such as that based on a statistical study of observed binary neutron stars in our Galaxy [107]. However, the detection of GW170817 by detectors of the horizon distance of $D_{\text{eff}} \approx 100$ Mpc in half a year observation with the duty cycle of $\sim 50\%$ suggests that the event rate of the binary neutron-star mergers may be $\sim 10^{-4}/\text{yr}$ in a Milky Way–equivalent galaxy [1]. Therefore, the merger rate estimated here is a reasonable value.

D. Radio flares

The (subrelativistic) merger ejecta sweep up the interstellar matter and form blast waves. In the shocked matter, the magnetic fields are amplified, and electrons are accelerated. This process will produce a synchrotron radio flare [108]. The ejecta discussed in this paper can be the source of the observable radio flares.

The radio flare will reach peak luminosity when the total swept-up mass approaches the ejecta mass [108]. Assuming that the interstellar matter is composed primarily of hydrogen and helium, the deceleration radius, R_{dec} , for spherical homologous ejecta is calculated [108–110], and then the deceleration time defined by $R_{\text{dec}}/\bar{v}_{\text{ej}}$ is given by

$$t_{\text{dec}} \approx 45 \text{ yr} \left(\frac{E_0}{6 \times 10^{50} \text{ erg}} \right)^{1/3} \left(\frac{n_0}{0.01 \text{ cm}^{-3}} \right)^{-1/3} \times \left(\frac{\bar{v}_{\text{ej}}}{0.15c} \right)^{-5/3}, \quad (4.6)$$

where n_0 is the number density of the interstellar matter (ISM) and $E_0 = M_{\text{ej}} \bar{v}_{\text{ej}}^2 / 2$ is the total kinetic energy of the ejecta. For $M_{\text{ej}} = 0.03 M_{\odot}$ and $\bar{v}_{\text{ej}} = 0.15c$,

$$E_0 = 6 \times 10^{50} \text{ erg} \left(\frac{M_{\text{ej}}}{0.03 M_{\odot}} \right) \left(\frac{\bar{v}_{\text{ej}}}{0.15c} \right)^2. \quad (4.7)$$

Thus, the radio flare associated with the ejecta is expected to reach the peak approximately at $\sim 45(n_0/0.01 \text{ cm}^{-3})^{-1/3}$ yr after the merger.

For the typical value of the ejecta velocity $\bar{v}_{\text{ej}} \sim 0.15c$, the peak flux for the observed frequency is obtained at the deceleration time described in Eq. (4.6). The peak flux for a given observed radio-band frequency ν_{obs} is estimated as [108]

$$\begin{aligned} F_{\nu} &\approx 190 \mu\text{Jy} \left(\frac{E_0}{10^{51} \text{ erg}} \right) \left(\frac{n_0}{0.01 \text{ cm}^{-3}} \right)^{(p+1)/4} \\ &\times \left(\frac{\epsilon_e}{0.1} \right)^{p-1} \left(\frac{\epsilon_B}{0.1} \right)^{(p+1)/4} \left(\frac{\bar{v}_{\text{ej}}}{0.15c} \right)^{(5p-7)/2} \\ &\times \left(\frac{D}{40 \text{ Mpc}} \right)^{-2} \left(\frac{\nu_{\text{obs}}}{1.4 \text{ GHz}} \right)^{-(p-1)/2}, \end{aligned} \quad (4.8)$$

where we assumed the power-law distribution of the electron's Lorentz factor with the power-law index $p = 2.5$ for deriving the specific value and ϵ_e and ϵ_B denote the energy fractions of accelerated electrons and magnetic field in the shock, respectively. Equation (4.8) is applicable as long as the observed frequency is higher than the typical synchrotron and self-absorption frequency at the deceleration time, t_{dec} . Equation (4.8) shows that the peak flux is high enough for the radio telescope to detect the signal, even if n_0 is not very high as $\sim 0.01 \text{ cm}^{-3}$ [111].

We note that the dynamical ejecta could have a velocity distribution in a broad range up to $\approx 0.8c$, and this fast component with the ejecta velocity $v_{\text{ej}} \gtrsim 0.5c$ could have appreciable mass of $\sim 10^{-5} - 10^{-4} M_{\odot}$ (i.e., the kinetic energy is $\sim 2 \times 10^{48} - 2 \times 10^{49}$ erg) [36]. Its deceleration time is much shorter as $\sim (1-2)(n_0/0.01 \text{ cm}^{-3})^{-1/3}$ yr. Therefore, the radio light curve arising from the dynamical ejecta is likely to have a broad peak [110]. The peak flux arising from this early fast component is estimated as

$$\begin{aligned} F_{\nu} &\approx 30 \mu\text{Jy} \left(\frac{E_{0,f}}{5 \times 10^{48} \text{ erg}} \right) \left(\frac{n_0}{0.01 \text{ cm}^{-3}} \right)^{(p+1)/4} \\ &\times \left(\frac{\epsilon_e}{0.1} \right)^{p-1} \left(\frac{\epsilon_B}{0.1} \right)^{(p+1)/4} \left(\frac{v_{\text{ej},f}}{0.5c} \right)^{(5p-7)/2} \\ &\times \left(\frac{D}{40 \text{ Mpc}} \right)^{-2} \left(\frac{\nu_{\text{obs}}}{1.4 \text{ GHz}} \right)^{-(p-1)/2}, \end{aligned} \quad (4.9)$$

where $E_{0,f}$ and $v_{\text{ej},f}$ denote the kinetic energy and velocity for the fast component. The peak time of the flux arising

from this component is earlier than the deceleration time estimated by Eq. (4.6) because the difference between the observer time and the time in the ejecta frame is significant for the ejecta with such high velocities. The rise rate of the radio flux is shallower than $\propto t^3$ due to the contribution of the shells with different velocities [110]. Depending on the ISM density and the velocity distribution, the radio signal can be detected, even far before the peak time described in Eq. (4.6) for GW170817. The detection of the radio flare at early times is quite important for proving the dynamical ejecta of the merger. Since the mass and velocity for the early component of the dynamical ejecta depend strongly on the neutron-star EOS (faster material is ejected for more compact neutron stars), the luminosity as a function of time will also carry information for the EOS.

The detection of the early radio signals reported by Refs. [111,112] is not likely to be associated with the subrelativistic mass ejection with $\bar{v}_{\text{ej}} \sim 0.2c$ unless $n_0 \gg 0.01 \text{ cm}^{-3}$. Note that the density inferred from the limit of the observation for the HI region is $< 10^{-2} \text{ cm}^{-3}$. Therefore, this early radio signal is likely to be associated with some relativistic mass ejection with $\bar{v}_{\text{ej}} \sim c$ [111,112]. We speculate that the radio flare associated with the mass ejection of fast motion with $v_{\text{ej}} \gtrsim 0.5c$ will be detected by subsequent observations in a few years.

E. Perspective for possible future events

If the inclination angle of the rotational axis of the binary orbital motion with respect to our line of sight were close to $\sim 90^\circ$, the observational properties of the electromagnetic counterparts of GW170817 would be significantly different from those of the electromagnetic counterparts of this event because lanthanide elements are likely to be present along our line of sight. If so, the electromagnetic counterpart would be much less luminous, and the time to reach the peak luminosity would be delayed because we could only observe the ejecta of high opacity $\kappa \sim 10 \text{ cm}^2/\text{g}$. For such events, the ratio of the effective distance, D_{eff} , to the luminosity distance, D , to the source should be larger than ~ 1.5 , and hence the SNR for the gravitational-wave observation would be smaller than that for GW170817 for a given value of D ; i.e., the observation would be less frequent. However, in the future for which the sensitivity of the gravitational-wave detectors is improved significantly, such edge-on events will be detected by the gravitational-wave detectors, and in such a forthcoming case, a macronova/kilonova, for which the feature is different from that of GW170817 even for the same mass of binary components, will be observed (see also Ref. [113]).

As discussed in Sec. III, the remnant for the merger in the GW170817 event would be a long-lived massive neutron star surrounded by a torus. However, this may be the case only for $m \lesssim 2.8 M_{\odot}$ even for the stiff EOS. For events with $m \gtrsim 2.8 M_{\odot}$, the remnant may be a black hole

surrounded by a torus. As described in Sec. III B, for this case, the ejecta could always be composed of neutron-rich matter with $Y_e \lesssim 0.2$. Then, the opacity of the ejecta should be high, $\kappa \sim 10 \text{ cm}^2/\text{g}$, and hence the peak time and peak luminosity of the electromagnetic counterparts could be significantly different from those for GW170817. When such a macronova/kilonova is discovered associated with a gravitational-wave detection for the merger of binary neutron stars, the results for the electromagnetic counterparts together with the total mass of the binary system will be used to constrain the neutron-star EOS.

As mentioned in Sec. IV B, the electromagnetic observation for GW170817 suggests that a remnant massive neutron star collapses to a black hole before a substantial fraction of its rotational kinetic energy is dissipated through the magnetic dipole radiation. However, for an event in which the total mass of a system (and, as a result, the mass of the remnant massive neutron star) is smaller than that for GW170817, the remnant massive neutron star may survive for a longer time scale of $\gtrsim 100 \text{ s}$. In such a case, a large fraction of its rotational kinetic energy may be released by the magnetic dipole radiation, leading to the acceleration of the ejecta to a relativistic speed. As a result, we expect a strong synchrotron radiation, which peaks at the radio bands, arising from the forward shock [99,100] and a magnetar-wind nebula producing the optical and x-ray emission [101]. In the future observation, this type of the event could be found for the merger of low-mass binary neutron stars. The observation of such an event will be also used to constrain the neutron-star EOS because we can obtain a lower bound for the maximum mass of rapidly rotating neutron stars. Thus, the future observations for a variety of the binary neutron-star mergers will significantly narrow down the possibility for the neutron-star EOS.

V. SUMMARY

In this paper, we attempt to interpret the observational results for the electromagnetic counterparts of GW170817 using the results of our numerical-relativity simulations performed so far. The characteristic features for the electromagnetic counterparts are their early peak time and high luminosity in the optical to IR bands. The numerical-relativity results indicate that a long-lived massive neutron star surrounded by a torus is a favored remnant for interpreting this event because only in the presence of such a strong neutrino emitter can the major ejecta component of sufficiently large mass of $\sim 0.03 M_\odot$ have a sufficiently high electron fraction of $Y_e \gtrsim 0.25$, avoiding the enhancement of the ejecta opacity. The long-lived massive neutron star also plays a role for ejecting an appreciable amount of material of fast motion. For getting such merger remnants, an EOS with a reasonably high value of M_{max} is required. No detection of a relativistic optical counterpart suggests a value of M_{max} approximately to be $2.15\text{--}2.25 M_\odot$.

As discussed in Sec. III B, if the remnant of the merger is a black hole surrounded by a torus, we may not have a strong emitter of neutrinos. If so, it would not reproduce the electromagnetic observational results of GW170817. However, it is not currently clear whether the torus is really a weak emitter of neutrinos or not. Some numerical experiments suggest that the torus surrounding a spinning black hole could be a strong emitter of neutrinos with the luminosity appreciably larger than 10^{52} erg/s , if the torus mass is sufficiently large. To date, we have not had detailed general relativistic radiation hydrodynamics simulations for such systems. We plan to perform simulations for this system in the near future.

Also, we plan to perform a variety of simulations fixing the chirp mass of $\mathcal{M} \approx 1.19 M_\odot$ but employing new EOS like in Ref. [95] and changing mass ratio, q , for a wide range. Our present study indicates that the merger remnant for the GW170817 event should be a strong emitter of neutrinos like a long-lived massive neutron star. To form a massive neutron star from binaries of total mass $\gtrsim 2.73 M_\odot$, a stiff EOS is necessary. This suggests that soft EOS like the SFHo EOS may be excluded. Generally speaking, EOS that produce a large-radius neutron star are suitable for forming a long-lived massive neutron star as the merger remnant. However, even in the case in which the typical radius is not very large (e.g., $\sim 11\text{--}12 \text{ km}$) as suggested by the analysis of the binary tidal deformability to GW170817, if the maximum-allowed mass for cold spherical neutron stars is appreciably larger than $2 M_\odot$ (say, $2.2 M_\odot$ [95]), a long-lived massive neutron star is likely to be the typical merger remnant. For exploring this possibility, we need more simulations employing a variety of neutron-star EOS.

ACKNOWLEDGMENTS

We thank Jim Lattimer, Brian Metzger, and Tsvi Piran for useful discussions during a long-term workshop ‘‘Electromagnetic Signatures of r-process Nucleosynthesis in Neutron Star Binary Mergers,’’ INT 17-2b, in Seattle. We also thank K. Ioka, K. Kashiyama, and K. Kawaguchi for helpful discussions. Numerical computation was performed on K computer at AICS (Projects No. hp160211 and No. hp170230), on Cray XC30 at cfca of National Astronomical Observatory of Japan, FX10 at Information Technology Center of the University of Tokyo, HOKUSAI FX100 at RIKEN, and on Cray XC40 at Yukawa Institute for Theoretical Physics, Kyoto University. This work was supported by Grant-in-Aid for Scientific Research (Grants No. 16H02183, No. JP16H06342, No. JP17H01131, No. 17H06361, and No. 15K05077) of JSPS and by a post-K computer project (Priority Issue No. 9) of Japanese MEXT. K. H. is supported by Flatiron fellowship at the Simons Foundation and Lyman Spitzer Jr. Fellowship.

APPENDIX: NOTE ON DYNAMICAL EJECTA MASS

Because our referee suggests we compare the backgrounds in general-relativistic radiation hydrodynamics simulations for the study of dynamical ejecta by different groups, we list several quantities for a specific model in Table IV. In this model, the SFHo EOS is employed, and each mass of the binary is $m_1 = m_2 = 1.35 M_\odot$. All the groups employ a mesh-refinement algorithm, but the location of the outer boundary along each axis and minimum grid spacing are different among different groups, in particular, between ours and other groups. The floor density has to be put in a dilute-density or vacuum region outside the neutron stars and merger remnant when using the conservative form of hydrodynamics in numerical simulations. Its choice is one of the crucial artificial points for accurately exploring the mass ejection during the merger process and is also likely to be different among four groups. Finally, most groups except for ours performed simulations simply using a leakage scheme without taking into account neutrino heating. The neutrino heating is crucial for exploring the values of the electron fraction and nucleosynthesis in the ejecta. Also, the difference in the treatments of neutrino physics affects the properties of the ejecta. According to Foucart *et al.* [114], the ejecta mass and the electron fraction of the polar ejecta could be changed by $\sim 20\%$ and $\gtrsim 50\%$ due to the treatment of neutrinos in the energy-integrated radiation transport scheme (specifically, the definition of the neutrino energy could affect the results). It should be also mentioned that the neutrino leakage scheme employed by us is different from other groups, all of which use a similar scheme. Currently, it is difficult to quantify the uncertainty caused by the neutrino treatment because of the lack of reliable results based on more physical neutrino transport schemes.

Table IV shows that the setup for the simulations is significantly different among four groups. The three groups except for ours located the outer boundaries at a region

fairly close to the center and estimated the ejecta mass essentially in the near zone. If a part of the ejecta component is produced by getting energy in a far region, e.g., by angular momentum transport due to tidal torque exerted by the central object and neutrino heating, the ejecta mass could be underestimated for the simulations with a small computational region (see also a discussion of Ref. [116]). It should be also noted that these groups estimated the ejecta mass before the spacetime in a corresponding region relaxes to a stationary state because the typical velocity of the dynamical ejecta is $v_{\text{ej}} \sim 0.2c - 0.25c$, i.e., $\approx 60 - 75$ km/ms, and the ejecta go through the outer boundaries or the surface of the flux integral at $\lesssim 10$ ms after the onset of merger. We note here that for estimating the ejecta mass we usually employ the condition of $u_t < -1$ or $hu_t < -1$, where u_t is the lower time component of the 4-velocity and h is the specific enthalpy. When we employ this method, the spacetime has to be stationary (a timelike Killing vector has to be present), but it is not clear whether the stationarity is well established at $\lesssim 10$ ms after the onset of merger.

On the other hand, we prepared a wider computational domain and calculated the ejecta mass by the direct volume integral at late time, i.e., at 20–30 ms after the onset of merger [40]. We note that for employing this method the computational region is wide enough ($L \gtrsim v_{\text{ej}} \times 30 \text{ ms} \sim 2000$ km) and the floor density is small enough (the total floor mass is much smaller than the ejecta mass for $L \lesssim 2000$ km). We then confirmed that the ejecta mass depends weakly on the time of the estimation. We caution that the ejecta mass depends strongly on the time of estimation, if we estimate it at $\lesssim 10$ ms after the onset of merger (see Fig. 1 of Ref. [40]); the estimation at earlier time results spuriously in a smaller ejecta mass of $< 0.01 M_\odot$.

Our numerical results indicate that the finer grid resolution results in smaller ejecta mass (see Table IV). Thus, in reality, the ejecta mass may be slightly smaller than

TABLE IV. Comparison of the ejecta mass for a model with the SFHo EOS and $m_1 = m_2 = 1.35 M_\odot$. Listed are locations of the outer boundary along each axis, L , the minimum grid spacing, Δx , floor density, presence or absence of neutrino heating (irradiation), and dynamical ejecta mass. The values in the parenthesis for the row of L denote the location where the information of the ejecta is extracted. “No description” means that no information is written on the corresponding point. In the unpublished work by Shibata, Hotokezaka, Kyutoku, and Sekiguchi, they constructed a piecewise polytropic EOS for the SFHo EOS and performed a purely hydrodynamics simulation as done in Ref. [36].

| Groups | L (km) | Δx (m) | Floor density (g/cm^3) | Neutrino heating | Ejecta mass (M_\odot) |
|-------------------------------------|------------|----------------|--|------------------|---------------------------|
| Sekiguchi <i>et al.</i> [40] | 10944 | 150 | 1.6×10^4 | Yes | 1.1×10^{-2} |
| Sekiguchi <i>et al.</i> [40] | 10240 | 250 | 1.6×10^4 | Yes | 1.3×10^{-2} |
| Sekiguchi <i>et al.</i> [40] | 10240 | 250 | 1.6×10^4 | No | 1.0×10^{-2} |
| Palenzuela <i>et al.</i> [115] | 750 | 230 | 6×10^5 | No | 3.2×10^{-3} |
| Bovard <i>et al.</i> [116] | 760 (300) | 215 | no description | No | 3.5×10^{-3} |
| Radice <i>et al.</i> [117] | 1512 (433) | 185 | no description | No | 3.5×10^{-3} |
| Shibata <i>et al.</i> (unpublished) | 2858 | 186 | 8.2×10^3 | No | 1.1×10^{-2} |

$0.011 M_{\odot}$ in our radiation-hydrodynamics implementation. Our numerical results also show that in the presence of neutrino heating the ejecta mass is increased by 30% (see Table IV). Thus, if other groups take into account this effect, their estimation for the dynamical ejecta mass may be increased.

To cross-check our result on the ejecta mass, we also performed a purely hydrodynamics simulation employing a piecewise polytropic EOS model for the SFHo EOS as done in Ref. [36] (see the last column of Table IV). For this case, the ejecta mass agrees broadly with that in Ref. [40]. This suggests that radiation hydrodynamics effects would play a subdominant role for determining the ejecta mass if it

is as large as $\sim 0.01 M_{\odot}$. However, these effects are likely to become appreciable when the mass of dynamical ejecta is small.

As found from the above discussion, obviously, comparison of the numerical results by different groups cannot be currently done in a well-defined manner because the computational setups are significantly different among them. In the future, we need comparison employing the same computational region, grid spacing, and floor density with the same neutrino physics. In the absence of such comparison works, it is safe to keep in mind that there is an uncertainty of a factor ~ 2 in the estimation of the dynamical ejecta mass.

-
- [1] B. P. Abbott *et al.*, *Phys. Rev. Lett.* **119**, 161101 (2017).
 [2] LIGO Scientific and VIRGO Collaborations, *Astrophys. J.* **848**, L12 (2017).
 [3] M. Tanaka *et al.*, [arXiv:1710.05850](https://arxiv.org/abs/1710.05850).
 [4] I. Arcavi *et al.*, *Nature (London)* **551**, 64 (2017).
 [5] E. Pian *et al.*, *Nature (London)* **551**, 67 (2017).
 [6] S. J. Smartt *et al.*, *Nature (London)* **551**, 75 (2017).
 [7] D. A. Coulter *et al.*, [arXiv:1710.05452](https://arxiv.org/abs/1710.05452).
 [8] M. R. Drout *et al.*, [arXiv:1710.05443](https://arxiv.org/abs/1710.05443).
 [9] B. J. Shappee *et al.*, [arXiv:1710.05432](https://arxiv.org/abs/1710.05432).
 [10] M. M. Kasliwal *et al.*, [arXiv:1710.05436](https://arxiv.org/abs/1710.05436).
 [11] M. Soares-Santos *et al.*, *Astrophys. J. Lett.* **848**, L16 (2017).
 [12] P. S. Cowperthwaite *et al.*, *Astrophys. J. Lett.* **848**, L17 (2017).
 [13] M. Nicholl *et al.*, *Astrophys. J. Lett.* **848**, L18 (2017).
 [14] S. Covino *et al.*, *Nat. Astron.* **1**, 791 (2017).
 [15] L.-X. Li and B. Paczyński, *Astrophys. J.* **507**, L59 (1998).
 [16] B. D. Metzger, G. Martinez-Pinedo, S. Darbha, E. Quataert, A. Arcones, D. Kasen, T. Thomas, P. Nugent, I. V. Panov, and N. T. Zinner, *Mon. Not. R. Astron. Soc.* **406**, 2650 (2010).
 [17] J. M. Lattimer and D. N. Schramm, *Astrophys. J.* **192**, L145 (1974).
 [18] D. Eichler, M. Livio, T. Piran, and D. N. Schramm, *Nature (London)* **340**, 126 (1989).
 [19] J. Barnes and D. Kasen, *Astrophys. J.* **775**, 18 (2013).
 [20] M. Tanaka and K. Hotokezaka, *Astrophys. J.* **775**, 113 (2013).
 [21] D. Kasen, N. R. Badnell, and J. Barnes, *Astrophys. J.* **774**, 25 (2013).
 [22] M. Tanaka *et al.*, [arXiv:1708.09101](https://arxiv.org/abs/1708.09101).
 [23] M. Shibata, *Phys. Rev. D* **60**, 104052 (1999).
 [24] M. Shibata and K. Uryū, *Phys. Rev. D* **61**, 064001 (2000).
 [25] LIGO Scientific and Virgo Collaborations, *Astrophys. J. Lett.* **848**, L13 (2017).
 [26] A. Goldstein *et al.*, *Astrophys. J. Lett.* **848**, L14 (2017).
 [27] V. Savchenko *et al.*, *Astrophys. J. Lett.* **848**, L15 (2017).
 [28] D. Lazzati, D. López-Cámara, M. Cantiello, B. J. Morsony, R. Perna, and J. C. Workman, *Astrophys. J.* **848**, L6 (2017).
 [29] O. Gottlieb, E. Nakar, T. Piran, and K. Hotokezaka, [arXiv:1710.05896](https://arxiv.org/abs/1710.05896).
 [30] T. Tauris *et al.*, *Astrophys. J.* **846**, 170 (2017).
 [31] T. W. Baumgrate, S. L. Shapiro, and M. Shibata, *Astrophys. J. Lett.* **528**, L28 (2000).
 [32] M. Shibata, *Numerical Relativity* (World Scientific, Singapore, 2016).
 [33] M. Shibata, K. Taniguchi, and K. Uryū, *Phys. Rev. D* **71**, 084021 (2005).
 [34] M. Shibata and K. Taniguchi, *Phys. Rev. D* **73**, 064027 (2006).
 [35] K. Hotokezaka, K. Kyutoku, H. Okawa, M. Shibata, and K. Kiuchi, *Phys. Rev. D* **83**, 124008 (2011).
 [36] K. Hotokezaka, K. Kiuchi, K. Kyutoku, H. Okawa, Y.-i. Sekiguchi, M. Shibata, and K. Taniguchi, *Phys. Rev. D* **87**, 024001 (2013).
 [37] K. Hotokezaka, K. Kiuchi, K. Kyutoku, T. Muranushi, Y.-i. Sekiguchi, M. Shibata, and K. Taniguchi, *Phys. Rev. D* **88**, 044026 (2013).
 [38] K. Takami, L. Rezzolla, and L. Baiotti, *Phys. Rev. D* **91**, 064001 (2015).
 [39] T. Dietrich, S. Bernuzzi, M. Ujevic, and B. Brügmann, *Phys. Rev. D* **91**, 124041 (2015).
 [40] Y. Sekiguchi, K. Kiuchi, K. Kyutoku, and M. Shibata, *Phys. Rev. D* **91**, 064059 (2015).
 [41] Y. Sekiguchi, K. Kiuchi, K. Kyutoku, M. Shibata, and K. Taniguchi, *Phys. Rev. D* **93**, 124046 (2016).
 [42] A. Steiner, M. Hempel, and T. Fischer, *Astrophys. J.* **774**, 17 (2013).
 [43] S. Banik, M. Hempel, and D. Bandyopadhyay, *Astrophys. J. Suppl. Ser.* **214**, 22 (2014).
 [44] A. Akmal, V. R. Pandharipande, and D. G. Ravenhall, *Phys. Rev. C* **58**, 1804 (1998).
 [45] N. K. Glendenning and S. A. Moszkowski, *Phys. Rev. Lett.* **67**, 2414 (1991).
 [46] A. Perego, S. Rosswog, R. Cabezón, O. Korobkin, R. Kaeppli, A. Arcones, and M. Liebendoerfer, *Mon. Not. R. Astron. Soc.* **443**, 3134 (2014).

- [47] F. Foucart, R. Haas, M. D. Duez, E. O'Connor, C. D. Ott, L. Roberts, L. E. Kidder, J. Lippuner, H. P. Pfeiffer, and M. A. Scheel, *Phys. Rev. D* **93**, 044019 (2016).
- [48] Y.-Z. Qian and S. E. Woosley, *Astrophys. J.* **471**, 331 (1996).
- [49] O. Korobkin, S. Rosswog, A. Arcones, and C. Winteler, *Mon. Not. R. Astron. Soc.* **426**, 1940 (2012).
- [50] S. Wanajo, Y. Sekiguchi, N. Nishimura, K. Kiuchi, K. Kyutoku, and M. Shibata, *Astrophys. J. Lett.* **789**, L39 (2014).
- [51] D. Kasen, R. Fernández, and B. D. Metzger, *Mon. Not. R. Astron. Soc.* **450**, 1777 (2015).
- [52] D. Kasen *et al.*, *Nature (London)* **551**, 80 (2017).
- [53] P. B. Demorest, T. Pennucci, S. M. Ransom, M. S. E. Roberts, and J. W. T. Hessels, *Nature (London)* **467**, 1081 (2010); J. Antoniadis *et al.*, *Science* **340**, 1233232 (2013).
- [54] J. S. Read, C. Markakis, M. Shibata, K. Uryu, J. D. E. Creighton, and J. L. Friedman, *Phys. Rev. D* **79**, 124033 (2009).
- [55] K. Kiuchi, K. Kawaguchi, K. Kyutoku, Y. Sekiguchi, M. Shibata, and K. Taniguchi, *Phys. Rev. D* **96**, 084060 (2017).
- [56] K. Kiuchi, Y. Sekiguchi, M. Shibata, and K. Taniguchi, *Phys. Rev. D* **80**, 064037 (2009).
- [57] A. Bauswein, O. Just, N. Stergioulas, and H. -Th Janka, [arXiv:1710.06843](https://arxiv.org/abs/1710.06843).
- [58] M. Shibata, K. Hotokezaka, K. Kiuchi, K. Kyutoku, and Y. Sekiguchi (to be published).
- [59] R. Fernández and B. D. Metzger, *Mon. Not. R. Astron. Soc.* **435**, 502 (2013).
- [60] B. D. Metzger and R. Fernández, *Mon. Not. R. Astron. Soc.* **441**, 3444 (2014).
- [61] R. Fernández, D. Kasen, B. D. Metzger, and E. Quataert, *Mon. Not. R. Astron. Soc.* **446**, 750 (2015).
- [62] O. Just, A. Bauswein, R. A. Pulpillo, S. Goriely, and H.-Th. Janka, *Mon. Not. R. Astron. Soc.* **448**, 541 (2015).
- [63] D. M. Siegel and B. D. Metzger, *Phys. Rev. Lett.* (2017).
- [64] J. Lippuner, R. Fernández, L. F. Roberts, F. Foucart, D. Kasen, B. D. Metzger, and Christian D. Ott, *Mon. Not. R. Astron. Soc.* **472**, 904 (2017).
- [65] S. Fujibayashi, K. Kiuchi, N. Nishimura, Y. Sekiguchi, and M. Shibata, [arXiv:1711.02093](https://arxiv.org/abs/1711.02093).
- [66] M. Shibata, K. Kiuchi, and Y. Sekiguchi, *Phys. Rev. D* **95**, 083005 (2017).
- [67] N. I. Shakura and R. A. Sunyaev, *Astron. Astrophys.* **24**, 337 (1973).
- [68] S. L. Shapiro and S. A. Teukolsky, *Black Holes, White Dwarfs, and Neutron Stars: The Physics of Compact Objects* (Wiley, New York, 1983).
- [69] J. F. Hawley, S. A. Richers, X. Guan, and J. H. Krolik, *Astrophys. J.* **772**, 102 (2013).
- [70] T. K. Suzuki and S. Inutsuka, *Astrophys. J.* **784**, 121 (2014).
- [71] J. M. Shi, J. M. Stone, and C. X. Huang, *Mon. Not. R. Soc. Astron.* **456**, 2273 (2016); G. Salvesen, J. B. Simon, P. J. Armitage, and M. C. Begelman, *Mon. Not. R. Soc. Astron.* **457**, 8578 (2016).
- [72] K. Kiuchi, K. Kyutoku, Y. Sekiguchi, and M. Shibata, [arXiv:1710.01311](https://arxiv.org/abs/1710.01311).
- [73] D. J. Price and S. Rosswog, *Science* **312**, 719 (2006).
- [74] K. Kiuchi, K. Kyutoku, Y. Sekiguchi, M. Shibata, and T. Wada, *Phys. Rev. D* **90**, 041502 (2014).
- [75] K. Kiuchi, P. Cerdá-Duran, K. Kyutoku, Y. Sekiguchi, and M. Shibata, *Phys. Rev. D* **92**, 124034 (2015).
- [76] J. Lippuner and L. Roberts, *Astrophys. J.* **815**, 82 (2015).
- [77] K. Kyutoku, K. Ioka, and M. Shibata, *Phys. Rev. D* **88**, 041503(R) (2013).
- [78] M. Tanaka, K. Hotokezaka, K. Kyutoku, S. Wanajo, K. Kiuchi, Y. Sekiguchi, and M. Shibata, *Astrophys. J.* **780**, 31 (2014).
- [79] K. Hotokezaka, R. Sari, and T. Piran, *Mon. Not. R. Astron. Soc.* **468**, 91 (2017).
- [80] K. Hotokezaka, S. Wanajo, M. Tanaka, A. Bamba, Y. Terada, and T. Piran, *Mon. Not. R. Astron. Soc.* **459**, 35 (2016).
- [81] J. Barnes, D. Kasen, M.-R. Wu, and G. Martínez-Pinedo, *Astrophys. J.* **829**, 110 (2016).
- [82] V. A. Villar *et al.*, [arXiv:1710.11576](https://arxiv.org/abs/1710.11576).
- [83] C. McCully *et al.*, *Astrophys. J. Lett.* **848**, L32 (2017).
- [84] N. R. Tanvir *et al.*, *Astrophys. J. Lett.* **848**, L27 (2017).
- [85] F. Foucart, E. O'Connor, L. Roberts, M. D. Duez, R. Haas, L. E. Kidder, C. D. Ott, H. P. Pfeiffer, M. A. Scheel, and B. Szilagyi, *Phys. Rev. D* **91**, 124021 (2015).
- [86] K. Kyutoku *et al.*, [arXiv:1710.00827](https://arxiv.org/abs/1710.00827).
- [87] M. Shibata, Y. Sekiguchi, and R. Takahashi, *Prog. Theor. Phys.* **118**, 257 (2007).
- [88] T. Damour, A. Nagar, and L. Villain, *Phys. Rev. D* **85**, 123007 (2012).
- [89] L. Wade, J. D. E. Creighton, E. Ochsner, B. D. Lackey, B. F. Farr, T. B. Littenberg, and V. Raymond, *Phys. Rev. D* **89**, 103012 (2014).
- [90] S. Bernuzzi, A. Nagar, T. Dietrich, and T. Damour, *Phys. Rev. Lett.* **114**, 161103 (2015).
- [91] M. Agathos, J. Meidam, W. Del Pozzo, T. G. F. Li, M. Tompitak, J. Veitch, S. Vitale, and C. Van Den Broeck, *Phys. Rev. D* **92**, 023012 (2015).
- [92] K. Hotokezaka, K. Kyutoku, Y. Sekiguchi, and M. Shibata, *Phys. Rev. D* **93**, 064082 (2016).
- [93] B. P. Abbott *et al.*, *Phys. Rev. Lett.* **119**, 141101 (2017).
- [94] J. M. Lattimer (private communication).
- [95] H. Togashi, K. Nakazato, Y. Takehara, S. Yamamuro, H. Suzuki, and M. Takano, *Nucl. Phys.* **A961**, 78 (2017).
- [96] J. M. Lattimer and M. Prakash, *Phys. Rep.* **621**, 127 (2016).
- [97] J. L. Friedman, J. R. Ipser, and L. Parker, *Astrophys. J.* **304**, 115 (1986).
- [98] V. M. Kaspi and A. M. Beloborodov, *Annu. Rev. Astron. Astrophys.* **55**, 261 (2017).
- [99] B. D. Metzger and G. C. Bower, *Mon. Not. R. Soc. Astron.* **437**, 1821 (2014).
- [100] A. Horesh, K. Hotokezaka, T. Piran, E. Nakar, and P. Hancock, *Astrophys. J.* **819**, L22 (2016).
- [101] B. D. Metzger and A. L. Piro, *Mon. Not. R. Astron. Soc.* **439**, 3916 (2014).
- [102] G. B. Cook, S. L. Shapiro, and S. A. Teukolsky, *Astrophys. J.* **424**, 823 (1994).
- [103] B. Margalit and B. D. Metzger, *Astrophys. J.* **850**, L19 (2017).
- [104] S. Goriery, *Astron. Astrophys.* **342**, 881 (1999).

- [105] C. Sneden, J. J. Cowan, and R. Gallino, *Annu. Rev. Astron. Astrophys.* **46**, 241 (2008).
- [106] K. Hotokezaka, T. Piran, and M. Paul, *Nat. Phys.* **11**, 1042 (2015).
- [107] C. Kim, B. B. P Perera, and M. A. McLaughlin, *Mon. Not. R. Astron. Soc.* **448**, 928 (2015).
- [108] E. Nakar and T. Piran, *Nature (London)* **478**, 82 (2011).
- [109] H. Takami, K. Kyutoku, and K. Ioka, *Phys. Rev. D* **89**, 063006 (2014).
- [110] K. Hotokezaka, S. Nissanke, G. Hallinan, T. J. W. Lazio, E. Nakar, and T. Piran, *Astrophys. J.* **831**, 190 (2016).
- [111] K. D. Alexander *et al.*, *Astrophys. J. Lett.* **848**, L21 (2017).
- [112] G. Hallinan *et al.*, [arXiv:1710.05435](https://arxiv.org/abs/1710.05435).
- [113] B. D. Metzger, [arXiv:1710.05931](https://arxiv.org/abs/1710.05931).
- [114] F. Foucart, E. O'Connor, L. Roberts, L. E. Kidder, H. P. Pfeiffer, and M. A. Scheel, *Phys. Rev. D* **94**, 123016 (2016).
- [115] C. Palenzuela, S. L. Liebling, D. Neilsen, L. Lehner, O. L. Caballero, E. O'Connor, and M. Anderson, *Phys. Rev. D* **92**, 044045 (2015).
- [116] L. Bovard, D. Martin, F. Guercilena, A. Arcones, L. Rezzolla, and O. Korobkin, [arXiv:1709.09630](https://arxiv.org/abs/1709.09630).
- [117] D. Radice, A. Perego, and F. Zappa, [arXiv:1711.03647](https://arxiv.org/abs/1711.03647).